RecA levels modulate biofilm development in *Acinetobacter baumannii*

Carly Ching[1,2], Merlin Brychcy[1], Brian Nguyen[1], Paul Muller[1], Alicyn Reverdy[1], Margaret Downs[1], Samuel Regan[4], Breanna Isley[1], William Fowle[1], Yunrong Chai[1], and Veronica G. Godoy[1*]

[1]Northeastern University, Department of Biology, Boston, MA, 02115

[2]Current address: Department of Biomedical Engineering, Boston University, Boston, MA, 02215

* Corresponding Author: Veronica G. Godoy, v.godoycarter@northeastern.edu

Abstract

Infections caused by *Acinetobacter baumannii,* a Gram-negative opportunistic pathogen, are difficult to eradicate due to the bacterium's propensity to quickly gain antibiotic resistances and form biofilms, a protective bacterial multicellular community. The *A. baumannii* DNA damage response (DDR) mediates the antibiotic resistance acquisition and regulates RecA in an atypical fashion; both $RecA^{Low}$ and $RecA^{High}$ cell types are formed in response to DNA damage. The findings of this study demonstrate that the levels of RecA can influence the development, formation and dispersal, of biofilms through the global biofilm regulator *bfmR*. RecA loss results in surface attachment and prominent biofilms, while elevated RecA leads to diminished attachment and dispersal. These findings suggest that the challenge to treat *A. baumannii* infections may be explained by the induction of the DDR, common during infection, as well as the delicate balance between maintaining biofilms in low RecA cells, and promoting mutagenesis and dispersal in high RecA cells. This study underscores the importance of understanding the fundamental biology of bacteria to develop more effective treatments for infections.

40 **Introduction**

41 *Acinetobacter baumannii* is an emerging Gram-negative opportunistic pathogen and one of the
42 ESKAPE pathogens, a group of bacteria responsible for most hospital-acquired infections(Rice, 2008).
43 *A. baumannii* outbreaks in hospitals are difficult to eradicate, due to increased multi-drug resistance
44 (MDR)(Peleg et al., 2008) and its ability to form biofilms(Eze et al., 2018). *A. baumannii* infections
45 are very dangerous to immunocompromised individuals, causing various illnesses, including
46 pneumonia, septicemia, and wound infections (Smith et al., 2007).

47

48 Generally, when gene products involved in antibiotic binding or processing on the chromosome are
49 mutated in a way that impacts their function, resistance can be acquired(Blair et al., 2014). One
50 response pathway underlying multidrug resistance (MDR) is the DNA damage response (DDR).
51 Mutagenesis results from the induction of error-prone DNA polymerase genes, which are part of the
52 DDR regulon(Cirz et al., 2007; Fuchs and Fujii, 2013). We have shown that in *A. baumannii*, RecA-
53 dependent induction of multiple error-prone polymerases in response to DNA damage leads to
54 clinically relevant antibiotic resistance (Norton et al., 2013). In *Escherichia coli* and many other
55 bacteria, the cells' main recombinase, RecA, and the global transcriptional repressor, LexA, manage
56 the DDR, also known as the SOS response(Little and Mount, 1982). In contrast, there is no known
57 LexA homolog in *A. baumannii*, indicating that the A. baumannii DDR circuitry is regulated differently
58 (Ching et al. 2017; Hare et al. 2014; MacGuire et al. 2014; Norton et al. 2013). Our lab has also shown
59 that in response to DNA damage, there are two RecA cell types, low *recA* expression ($RecA^{Low}$) and
60 high *recA* expression ($RecA^{High)}$, regulated by a 5'untranslated region in the *recA* transcript (Ching et
61 al., 2017; MacGuire et al., 2014).

62

63 Bacterial cells within biofilms are often less sensitive to chemical and physical challenges, including
64 antibiotics (Anderl and Franklin, 2000; Singh et al., 2016). Like many biological processes, the biofilm
65 cycle in *A. baumannii* is not fully understood, although key biofilm genes are known, including the
66 biofilm master regulator gene *bfmR* that controls adhesive *csu* pili and genes important for virulence
67 and desiccation tolerance(Farrow et al., 2018; Tomaras et al., 2008, 2003). It is also known that genes
68 encoding Bap protein and efflux pumps are important for biofilms(Brossard and Campagnari, 2012;
69 He et al., 2015; Loehfelm et al., 2008; Tomaras et al., 2008, 2003). The BfmR response regulator is
70 part of a two-component system (BfmRS) that results in BfmR phosphorylation (Farrow et al., 2018;
71 Geisinger and Isberg, 2015; Russo et al., 2016; Tomaras et al., 2008; Wang et al., 2018). There may
72 be additional factors regulating *bfmR* expression and it is unknown whether de-repression by
73 phosphorylated BfmR, with lower affinity for its operator site(Draughn et al., 2018), is sufficient for
74 induction. The *A. baumannii* biofilm extracellular matrix contains poly-ß-(1-6)-*N*-acetyl-glucosamine,
75 mannose and extracellular DNA(Bales et al., 2013; Choi et al., 2009; Hardouin et al., 2014; Sahu et
76 al., 2012).

77

78 In brief, the DDR and the biofilm cycle are two crucial pathways that bacteria use for survival under
79 stressful environmental conditions and there is evidence suggesting a link between these two
80 pathways(Linares et al., 2006; Takajashi et al., 1995). The mechanisms linking the DDR and biofilms
81 vary between bacterial species. For example, in *Streptococcus mutans*, *Escherichia coli* (Costa et al.,
82 2014; Inagaki et al., 2009), and *Clostridium difficile* (Walter et al., 2015), there is a direct correlation
83 between DDR and biofilm formation in which both pathways are induced in response to environmental
84 signals. However, we showed that during *Bacillus subtilis* biofilm development, induction of the DDR,
85 measured by levels of oxidative stress and gene expression of a *lexA* -dependent gene (not *recA* or *lexA*
86 directly), shuts off biofilm matrix genes (Gozzi et al., 2017). This suggested an inverse correlation

87 between DDR and biofilm formation in which DDR signaling complements the biofilm cycle; DDR-
88 induced cells could leave the biofilm to search for new niches. Altogether, the varied relationships
89 between DDR and the biofilm cycle are intriguing and show that cells have established different ways
90 to balance these strategies, which could have downstream effects in treatment and clinical practices.

91

92 Here, we demonstrate that DDR and the biofilm cycle also intersect in *A. baumannii*. We show that the
93 loss of RecA in *A. baumannii* results in increased cell-to-surface adherence, in part due to elevated
94 expression of *bfmR* with a concomitant increase in Csu pili. We further identify the novel regulation
95 of *bfmR* through the RecA-dependent UmuDAb gene product. UmuDAb is in the same family as LexA
96 and regulates some of the DDR genes in *A. baumannii* (Hare et al., 2014). We observed that DNA -
97 damaged biofilms shut off gene expression of the attachment pili coded by *csuAB* and turn on *recA*,
98 allowing for cell dispersal. The observed inverse relationship between DDR and biofilm formation
99 may lead to a heterogeneous cell population combining physical (biofilm) and genetic (elevated
100 mutagenesis) protection to environmental challenges, including antibiotics.

101

102 **Results**

103 **Loss of RecA promotes biofilms in *A. baumannii***

104 *A. baumannii* ATCC 17978 Δ*recA* cells (*recA*::km, Table S1 (Aranda et al., 2011)) grown in standard
105 LB medium and shaking conditions consistently displayed observable surface attachment on the sides
106 of glass tubes (Fig. 1A, red arrow). In comparison, the parental wild-type strain had little to no surface
107 attachment (Fig. 1A). Intriguingly, this observation suggested that *A. baumannii* Δ*recA* cells form a
108 more prominent biofilm than parental WT cells. Since the lack of RecA can presumably affect bacterial

109 growth (Cox et al., 2008), we first performed growth measurements of free-living planktonic WT and
110 Δ*recA* cells. We also measured growth in Δ*recA* cells complemented with a low-copy plasmid,
111 pNLAC1(Luke et al., 2010), containing *recA* under its own promoter (Ching et al., 2017) (Δ*rec*A
112 (pNLAC1-*recA*), Table S1), which we will refer to as the complemented Δ*recA* mutant or Δ*recA*-c.
113 We observed a slight growth disadvantage in Δ*recA* cells when the starting inoculum size was $<10^7$
114 cells that was rescued by the extrachromosomal copy of *recA* (Fig S1A & B). Our result is largely
115 consistent with a previous report that the Δ*recA* strain showed no noticeable growth defects compared
116 to the parental WT strain(Aranda et al., 2011).

117

118 We next assayed pellicle biofilm formation (formed at the air-liquid interface) of Δ*recA* and WT cells,
119 as indicated in materials and methods. WT cells did not form a visible pellicle (Fig. 1B, left) at 24 hrs
120 while Δ*recA* cells (Fig. 1B, middle) formed a visible and opaque pellicle as early as 24 hrs. At 48 and
121 72 hrs, the WT cells formed a smooth pellicle and with striations while the Δ*recA* pellicle was thicker
122 and granular on the surface (Fig. S2). Cell surface attachement along the sides/bottom of wells of
123 pellicle biofilms of WT and Δ*recA* strains containing the empty plasmid, along with the Δ*recA*-c strain,
124 was measured by Crystal Violet staining. We observed a significant increase in surface-attached cells
125 in Δ*recA* biofilms at 24 hrs compared to WT cells (Fig. 1C). At 24 hrs, pellicle formation of the
126 complemented strain was not significantly different than the parental strain (Fig 1B, right), and the
127 surface architecture was similar to WT (Fig. S2). These data suggest that the loss of RecA leads to a
128 increased biofilm formation.

129

130 Colony biofilm formation is indicated by growth at the air-surface interface (Vlamakis et al., 2013).
131 Typically, robust colony biofilms have more wrinkling surface architecture due to differential cell

132 death and mechanical forces due to increased extracellular matrix (Asally et al., 2012). Thus, we grew
133 colony biofilms on solid medium plates containing Congo red and Coomassie brilliant blue, dyes that
134 detect changes in biofilm matrix components (Ghodke et al., 2019; Surgalla and Beesley, 1969). At 48
135 hrs, the Δ*recA* colony biofilm had differential coloring to that of the WT and complemented strain,
136 indicative of increased biofilm matrix production (Fig 1D). We noticed that the Δ*recA* colony biofilms
137 also had decreased diameter size throughout the length of the experiment. Notably, the complemented
138 Δ*recA* colony is similar in size to WT but with an intermediate coloration (Fig. 1D). We have
139 previously observed partial complementation of colony biofilm phenotypes with plasmid -borne
140 ectopic gene copies, possibly due to the sensitivity of the process to gene dosage (Ching et al., 2018).
141 The data obtained from these experiments suggest that the Δ*recA* strain forms robust colony biofilms.
142

143 **The inverse relationship between RecA and biofilm is not exclusive to *A. baumannii* ATCC 17978**

144 To assess whether this finding was exclusive to *A. baumannii* ATCC 17978, we used a transposon
145 derivative of *A. baumannii* AB5075 in which the transposon is inserted approximately in the middle of
146 the RecA open reading frame (ORF) (Gallagher et al., 2015) (Table S1). *A. baumannii* AB5075 is a
147 highly virulent clinical isolate (Jacobs et al., 2014). For pellicle biofilms at 48 hrs, the AB5075
148 *recA::Tn* mutant had significantly increased cell adherence compared with the parental strain (Fig.
149 S3A). Furthermore, the AB5075 *recA::Tn* colony biofilm is also smaller than the parental strain and
150 displays differences in colony morphology, including changes in opacity and striations on the edge
151 (Fig. S3B). These data suggest that the observation that RecA negatively impacts biofilm development
152 is not exclusive to the ATCC 17978 strain.

153 **RecA modulates the biofilm matrix in *A. baumannii***

154 Since Δ*recA* cells form prominent biofilms, we were curious to visually observe differences between
155 Δ*recA* and WT biofilms, especially regarding the extracellular matrix. We thus analyzed Δ*recA* and
156 WT pellicle biofilms by scanning electron microscopy (SEM). To observe pellicle biofilms from the
157 WT and Δ*recA* strains we used a fixing procedure that takes advantage of cationic dyes binding to
158 negatively charged polysaccharides that preserves them for imaging (Erlandsen et al., 2004). We
159 observed noticeable differences between the matrix and biofilm structures of the WT and Δ*recA* strains
160 (Fig. 2A). At 24 hrs, WT cells have some matrix and connections between cells, while Δ*recA* cells
161 were embedded in an observable thick matrix (Fig. 2A). To determine and quantify whether the
162 differences in the biofilm matrix between the WT and Δ*recA* strains were partially due to changes in
163 polysaccharides, total extracellular matrix was extracted from stationary phase cells and carbohydrate
164 content was measured. Δ*recA* cells had a nearly 3-fold increase in total carbohydrates compared the
165 WT cells (Fig. S4). The complemented strain, Δ*recA*-c, had a similar carbohydrate level to WT cells
166 (Fig. S4). It is possible that in addition to increased sugar matrix content we may also be visualizing
167 other phenomena, such as increased pili, which led to further investigation below.

168

169 **Δ*recA* surface-attached cells withstand antibiotic treatment better**

170 Biofilms have been noted to protect bacteria from antibiotic exposure (Anderl and Franklin, 2000;
171 Singh et al., 2016). To determine whether there were any differences in the antibiotic susceptibility of
172 the WT and Δ*recA* biofilms compared to planktonic cells, surface-attached WT and Δ*recA* biofilms
173 were treated with the bactericidal aminoglycoside gentamicin. First, we determined the MIC of

174

175 amicin for exponentially growing planktonic cells in YT medium and found it to be the same for both
176 WT and Δ*recA* cells (1.88 µg/mL, error within 2-fold). Aranda *et al*. determined the MIC of planktonic
177 cells to Amikcin and Tobramycin, both aminoglycosides, and reported that these were also the same
178 for the WT and Δ*recA* strains (1.5 µg/mL and 0.38 µg/mL, respectively) (Aranda et al., 2011).

179

180 To assess whether biofilms withstood gentamicin exposure differently to planktonic cells, the spent
181 growth medium from 72 hr pellicle biofilms were removed, the wells were washed to eliminate non-
182 attached cells and gentamicin was added in fresh growth medium at different concentrations, and wells
183 were incubated for 24 hrs. After exposure to gentamicin, the growth medium and non-attached cells
184 were removed, and Crystal Violet staining was performed as before. The data are presented as the
185 percentage of untreated biofilms of each respective strain. For the Δ*recA* strain, the percentage of
186 surface-attached cells remaining after antibiotic treatment plateaus above 50% relative to no treatment
187 after exposure to 0.47–15 µg/mL of gentamicin (Fig. 2C), representing over 3-fold excess of Δ*recA*
188 surface-attached cells compared to WT (at 15 µg/mL the percentage of WT surface-attached cells
189 decreases to ~16% relative to no treatment). This suggests that that Δ*recA* withstood antibiotic
190 exposure better (Fig. 2B).

191 To determine if the remaining surface-attached cells were viable, we directly measured the viability of
192 surface-attached cells from pellicle biofilms of WT and Δ*recA* strains containing the empty plasmid,
193 along with the Δ*recA*-c strain, with and without gentamicin treatment, by plating for viable cells
194 (CFUs). We found that with gentamicin exposure (15 ug/mL), the Δ*recA* strain had ~ 5-fold increase
195 in percent survival compared to the WT strain, while the complement had similar survival to WT (Fig.
196 2D).

197 **Increasing RecA diminishes biofilm formation**

198 Together, our data suggest that there is an inverse relationship between RecA and biofilm development
199 in *A. baumannii.* To further test this relationship, we artificially increased RecA levels in WT cells and
200 expected that a RecA overproducing strain would form poor biofilms with fewer surface-attached cells
201 than WT or Δ*recA* biofilms. Thus, we introduced the plasmid -borne copy of *recA* under its own
202 promoter (pNLAC1-*recA,* Table S1) into the WT strain, which we refer to as $recA^{++}$ (Table S1). We
203 first measured the intracellular RecA concentration of $recA^{++}$ relative to the WT strain. To do this, we
204 purified *A. baumannii* RecA and *E. coli* RecA to test whether an antibody raised against *E. coli* RecA
205 recognizes *A. baumannii* RecA equally well. There was no difference between the detection of the *E.*
206 *coli* RecA or *A. baumannii* RecA for the antibody (Fig. S5A&B). Using semi-quantitative Western
207 blotting, we found that the relative level of RecA in $recA^{++}$ cells was between 3- to 5-fold higher than
208 WT in both basal and DNA-damage inducing conditions than the parental strain (Fig. S4C). We
209 calculated that after DNA damage, RecA relative levels in the WT strain increased by ~3-fold relative
210 to basal conditions. Thus, $recA^{++}$ at basal conditions has similar levels of RecA as the WT strain treated
211 with 10X MIC of ciprofloxacin (Fig. S5C). The $recA^{++}$ strain grown in planktonic conditions had a
212 slight growth defect, similar to Δ*recA* cells (0.15X slower doubling time than WT based on growth
213 curves) (Fig. S1 C&D). We observed that $recA^{++}$ biofilms had significantly less surface-attached cells
214 compared to the WT and Δ*recA* biofilms, but still above the baseline reading of a control empty stained
215 well (0.082 +/- 0.005) (Fig 3A).

216

217 **RecA levels influence surface attachment**

218 Since planktonic shaking cells for Δ*recA* and $recA^{++}$ cells is largely consistent with a previous report
219 that the Δ*recA* strain showed no noticeable growth defects compared to the parental WT strain (Aranda
220 et al., 2011) (Fig. S1) in the conditions tested, we concurrently measured biofilm attachment and

221 bacterial growth during the first 13 hours of static growth conditions. We inferred that any differences
222 in biofilms due to growth would be clear at the early stages of biofilm formation while there may be
223 active cell division. To do this, we setup biofilms as indicated in Materials and Methods and measured
224 surface attachment while also determining colony forming units (CFUs) of the whole well combining
225 attached and non-attached cells from 0-13 hrs at regular intervals. Strikingly, at 6 hrs we detected an
226 increase in surface-attached cells for Δ*recA* biofilms compared to WT and *recA*$^{++}$, which both showed
227 little attachment (Fig. 3B). The CFU counts were comparable for the strains (Fig. 3C). These data show
228 that Δ*recA* cells attach to surfaces earlier than WT or the *recA*$^{++}$ strains, as our previous assays
229 suggested (Fig. 1B). This also demonstrates that our findings for biofilm formation are directly
230 comparable and not, in part, due to growth differences. In this experiment, as well as in those one
231 shown previously (Fig. 1B), strains contained the empty plasmid (pNLAC1; Table S1) for direct
232 comparison to the complemented strain. We observed that regardless of pNLAC1 (Fig. 3B, C) Δ*recA*
233 forms robust biofilms, while WT and *recA*$^{++}$ do not. Overall our data indicates an inverse relationship
234 between RecA and biofilm development.

235

236 **RecA levels influence the density of attachment pili**

237 Because Δ*recA* cells attached to surfaces faster than WT or *recA*$^{++}$ (Fig. 3A-C), we wanted to
238 investigate whether Δ*recA* cells had more surface pili to permit attachment. Csu pili are involved in
239 cell adherence in *A. baumannii* biofilms (Gaddy and Actis, 2009; Pakharukova et al., 2018; Rumbo-
240 Feal et al., 2013; Tomaras et al., 2003). To investigate this, we imaged the Δ*recA*, WT and *recA*$^{++}$
241 strains from saturated cultures using transmission electron microscopy (TEM). Remarkably, Δ*recA*
242 cells displayed a higher density of surface pili than WT or *recA*$^{++}$ cells (Fig. 3D). To determine whether
243 we were observing, in part, Csu pili, we performed a Western blot to detect CsuAB protein from both

244 purified pili (Fig. 3E) and total cell extracts (Fig. 3F) and detected a strong signal for CsuAB pili in
245 Δ*recA* cells.

246

247 We next constructed a plasmid containing the promoter of the *csuAB* operon fused to *gfp* (P_{csuAB}-*gfp*),
248 which was introduced into Δ*recA*, WT, and $recA^{++}$ strains. Fluorescence measurements of statically
249 grown cells in YT medium showed that the reporter fluorescence intensity in Δ*recA* was consistently
250 higher compared to WT and $recA^{++}$, with $recA^{++}$ being consistently the lowest (Fig. 4A). Quantification
251 of fluorescence of single cells (Fig. 4B) shows significantly elevated average fluorescence in Δ*recA*
252 cells compared to $recA^{++}$ or WT. Notably, $recA^{++}$ fluorescence is significantly lower than WT (Fig.
253 4B). Our subsequent effort was to quantify the expression levels of *csu* pili genes in biofilm -dwelling
254 cells. Although the qPCR data suggested a higher trend in *csuA* expression in Δ*recA*, the results were
255 deemed statistically insignificant due to the presence of noise. This is likely due to the components in
256 the pellicle samples that may either inhibit PCR, result in poorer mRNA sampling, or due to the
257 inherent heterogeneity of biofilm -dwelling cells (Werner et al., 2004). Nevertheless, in stationary cells,
258 *csuAB* expression is ~80-fold higher in *A. baumannii* Δ*recA* and lower in $recA^{++}$ compared to WT cells
259 (Fig. 4C). In summary, our data indicate that Δ*recA* cells have deregulated CsuAB pili.

260

261 **RecA and *csuAB* expression are inversely correlated in DNA-damaged biofilm pellicles**

262 Due to the absence of a LexA homolog in *A. baumannii*, it is possible that RecA may serve different
263 regulatory roles, as has been previously suggested (Hare et al., 2014). Our results suggested that
264 elevated levels of RecA would lead to decreased CsuAB pili (Figs. 3-4). Thus, we hypothesized that
265 *csuAB* expression would decrease in biofilm cells upon treatment with a DNA damaging agent, which
266 increases RecA. To test this and monitor both RecA and *csuAB* expression, we constructed a plasmid

267 -borne transcriptional reporter of Csu genes (Fig. 4) (P_{csuAB}-*mCherry*), that was introduced into an *A.*
268 *baumannii* strain containing a chromosomal P_{recA}-*gfp* reporter (Ching et al. 2018). 48 hr pellicle
269 biofilms of the double reporter strain were treated with 0.5X MIC of ciprofloxacin (Cip), which induces
270 the DDR but does not kill cells (MacGuire et al., 2014), for an additional 48 hrs. The biofilm pellicles
271 were examined by confocal microscopy to observe differences in gene expression, and in biofilm
272 thickness.

273 In untreated biofilms (Fig. 5A), most cells had moderate to high expression of the P_{csuAB}-*mCherry* pili
274 reporter with few expressing P_{recA}-*gfp* (Fig. 5A). In comparison, cells isolated from Cip-treated
275 biofilms showed dramatic changes (Fig. 5B). Most of the DNA-damaged biofilm cells were fluorescing
276 GFP, an indication of RecA induction, with few cells expressing *mCherry*. There appeared little to no
277 overlap in gene expression between the two reporters, suggestive of mutually exclusive cell types.
278 Moreover, since mCherry and GFP have similar stability (Shaner et al., 2005), they are directly
279 comparable; the gene expression difference is not due to the fluorescence reporters. Most treated cells
280 were also elongated, as cell division inhibition is a common feature of DDR induction (Kreuzer, 2013)
281 that also happens in *A. baumannii*, as we have previously shown (Ching et al., 2017). Moreover, and
282 notably, the untreated pellicles showed high cell density and had a greater thickness (28 µm) than the
283 treated pellicles (22 µm), suggesting that biofilm dispersal occurred in response to DNA damage
284 treatment. It is unlikely that thinning is due to cell death by the Cip treatment since we used sub-MIC
285 levels of Cip. Our data suggest that RecA negatively influences the expression of *Csu* pili genes,
286 necessary for the expression of the Csu pili machinery and biofilm formation.

287

288 **RecA modulates *bfmR* expression**

289 Csu pili regulation depends on BfmR, a key regulator of biofilm formation in *A. baumannii* (Tomaras
290 et al., 2008). Increased Csu pili in Δ*recA* suggested either higher *bfmR* expression or a more active
291 BfmR. To test whether *bfmR* was differentially expressed in the Δ*recA*, WT, and *recA*$^{++}$ strains we
292 tracked a plasmid borne fluorescent reporter containing the promoter of the *bfmR* operon fused to
293 *mKate2* (P_{bfmR}-*mKate2*) over time. We found that *bfmR* expression is higher in Δ*recA*, but not in *recA*$^{++}$,
294 compared to WT (Fig. 6A). These results suggest that RecA levels manage *bfmR* expression that in
295 turn controls Csu pili.

296

297 **UmuDAb, a RecA-dependent transcription factor, regulates BfmR**

298 While *A. baumannii* lacks LexA, UmuDAb (A1S_1389), is a known repressor of some, but not all,
299 DDR genes(Hare et al., 2014). Notably, UmuDAb has a typical helix-turn-helix DNA binding motif
300 at the amino-terminal end that is cleaved by the activated RecA nucleoprotein filament, RecA*, in a
301 way believed to be to that of LexA and other proteins within the same family (Draughn et al., 2018;
302 Hare et al., 2013). Cleavage of UmuDAb by RecA* provides a plausible mechanistic explanation for
303 the observations that high RecA levels (i.e. low full-length UmuDAb) lead to biofilm dispersal. Thus,
304 we hypothesized that UmuDAb may serve as a RecA-dependent regulator of biofilm development.

305

306 We constructed an Δ*umuDAb* strain as previously done (Norton et al., 2013) and tested for biofilm
307 formation. We found that the Δ*umuDAb* strain formed significantly weaker biofilms than any other
308 strain previously studied in pairwise comparisons (Fig 6B). In fact, Δ*umuDAb* formed significantly
309 less biofilm than *recA*$^{++}$ (Fig. 6B). Consistent with this observation, TEM showed no visible pili on the
310 surface of Δ*umuDAb* cells (Fig 6C). Furthermore, we detected almost no *bfmR* expression in Δ*umuDAb*
311 *bfmR* reporter cells compared to WT (Fig 6A). Contrary to the known UmuDAb repressor
312 function(Hare et al., 2014; Witkowski et al., 2016), our findings suggest that UmuDAb has a positive

313 effect on *bfmR* and consequently on Csu pili. Indeed, we have biochemical evidence that full-length
314 UmuDAb binds to the *bfmrR* promoter, while the cleaved version does not (Fig. S6A). Our group is
315 currently further investigating the mechanistic details by which UmuDAb performs this function.
316 Overall, our data suggest a genetic model in which *A. baumannii* biofilm development depends on
317 RecA, UmuDAb, BfmR, and CsuAB (Fig. 6D, expanded upon in discussion). To test this genetically,
318 we designed a plasmid-based arabinose -inducible CRISPRi system and knocked down *recA* in WT,
319 Δ*umuDAb,* Δ*bfmR* and Δ*csuD*(Moon et al., 2017) cells (Fig. S6B). We then compared the pellicle
320 biofilm formation between these strains. As expected, when *recA* was knocked down in WT cells, there
321 was a significant increase in biofilm compared to WT cells with a nonsense single guide RNA (Fig.
322 6E). Furthermore, and as expected, knocking down RecA in each of Δ*umuDAb,* Δ*bfmR* and Δ*csuD*
323 strains, did not increase biofilms (Fig 6E).
324

325 **Discussion**

326 Bacteria largely exist in the environment as biofilms (Costerton et al., 1995). Generally, cells in
327 biofilms have different characteristics and gene expression profiles from their planktonic counterparts.
328 Here, we find that in *A. baumannii,* levels of RecA, a key DDR gene product, influences biofilm
329 development in both ATCC 17978 (Figs. 1-6) or AB5075 (Fig. S3) strains. Our data also show that
330 cells lacking *recA* produce robust biofilms (Fig. 1). Importantly, Δ*recA* biofilms on an abiotic surface
331 expected to be more resilient (Fig. 2) and a higher fraction of cells remain viable after antibiotic
332 treatment (Table 1) compared to the parental strain, providing additional evidence to the concept that
333 biofilms protect cells from antibiotic exposure (Anderl and Franklin, 2000; Singh et al., 2016). Thus,
334 recurring *A. baumannii* infections may be the product of cells remaining adhered to equipment surfaces
335 or implanted devices.

336 We found that RecA levels influence biofilm formation through Csu pili. Δ*recA* cell adherence depends
337 on higher *csuAB* and increased Csu pili compared to either the WT or the *recA*$^{++}$ strains (Figs. 3, 4).
338 Our results further suggest that *csuAB* expression is due to the induction of *bfmR* (Fig. 6). It has been
339 previously shown that *bfmR* and *csuAB* expression are higher in biofilm cells (Rumbo-Feal et al., 2013),
340 consistent with our findings.

341 Aranda *et al.* phenotypically characterized the *ΔrecA* insertional mutant used in this study. Free-living
342 *ΔrecA* cells had decreased survival during heat shock, desiccation, UV, and certain antibiotic
343 treatment(Aranda et al., 2011). Importantly, the *ΔrecA* strain had much lower pathogenicity in a mouse
344 model, indicating its importance in this process (Aranda et al., 2011). These results demonstrate the
345 significance of RecA in survival and virulence in planktonic cells. However, our findings demonstrate
346 the importance of investigating both biofilm and free-living states. For example, it has been shown that
347 strong *A. baumannii* biofilm formers are less frequently antibiotic-resistant, consistent with having
348 lower levels of RecA and subsequently mutagenesis (Wang et al., 2018). Additionally, planktonic cells
349 more readily gain higher level antibiotic resistance compared to biofilm cells during exposure to
350 ciprofloxacin (Santos-Lopez et al., 2019). Moreover, biofilm cells were more eradication-resistant
351 (Wang et al. 2018), again consistent with the observation that Δ*recA* surface-attached cells are more
352 difficult to eliminate with antibiotics (Fig. 2, and Table 1). This could be because certain antibiotics
353 have lowered penetration of biofilms (Anderl and Franklin, 2000; Singh et al., 2016) and there is a
354 nutrient gradient within the biofilm that leads to different metabolic states of biofilm cells (Werner et
355 al., 2004). Other explanations include an increase in antibiotic efflux in the biofilm conditions or that
356 the surface of the bacterium is very different in biofilms, and the antibiotic does not interact as
357 efficiently.
358

359 Our findings have significant implications for understanding *A. baumannii* survival to antibiotic
360 treatment and possibly antibiotic resistance. We show that upon DNA damage, the DNA damage
361 response is induced, leading to the induction of *recA* with simultaneous shutoff of biofilm genes,
362 leading to thinner biofilms (Fig. 5). We have observed that this occurs through lowered *bfmR* and
363 *csuAB* expression upon elevated RecA levels. Quantification of RecA upon DNA damage, and in
364 *recA*$^{++}$ cells, demonstrates how sensitive the biofilm gene expression is to a change in RecA levels
365 (Figs. S4, 1-3). This may be due to UmuDAb sensitivity to cleavage by RecA* (Hare et al., 2013). Our
366 evidence suggests that full-length UmuDAb is an inducer of *bfmR* and of biofilm formation (Fig. 6 and
367 supplementary Fig. S6B). A summary and model of genes, supported by our data, is shown in Fig. 6D.
368 Based on previous findings, we have observed two of RecA cell types, high and low, in planktonic
369 cells (Ching et al., 2017; MacGuire et al., 2014), and there may also be heterogeneity in RecA levels
370 among cells in biofilms. Thus, within a biofilm, the RecA^{Low} cells maintain biofilms with low
371 mutagenic potential, while RecA^{High} cells with high mutagenic potential (Norton et al., 2013) can
372 disperse and search for new niches. This observed inverse relationship can allow the population to
373 combine physical (biofilm) and genetic (elevated mutagenesis) protection to environmental challenges,
374 including antibiotic exposure in a host.

375

376 Overall, we have identified an inverse relationship between the DDR and biofilm development in *A.*
377 *baumannii.* While a similar anti-correlation was observed in *B. subtilis*, *A. baumannii* has a unique
378 DDR that it is not a canonical LexA-dependent SOS system. Thus, our findings provide further insights
379 on LexA-independent DDRs. Here, we uncover different underlying regulatory pathways and genes
380 mediating this inverse relationship. Specifically, the *Gozzi et al* paper does not test RecA directly, and
381 the mechanism is through the accumulation of reactive oxygen species, which induce the canonical
382 DDR and genes known to be in the LexA -dependent regulon(Gozzi et al., 2017). We show that

383 different levels of RecA govern biofilm genes and pili in a LexA-independent system. The direct
384 relationship between RecA and pili has not been reported and notably we have expanded on the RecA-
385 dependent regulon in *A. baumannii*. Although there may be by convergent evolution of the same
386 approach (biofilm and DNA damage responses have mutual exclusivity), we reveal a fundamentally
387 different approach in distantly related bacteria (Gram-negative vs Gram-positive, nonpathogenic vs
388 pathogen).

389

390 These results demonstrate the complexity of treating pathogens with a DDR that do not follow the
391 paradigm, such as *A. baumannii* (Ching et al., 2017; MacGuire et al., 2014). Previous work has
392 highlighted the potential for clinical RecA inhibitors to potentiate the effect of antibiotics while
393 hindering antibiotic resistance acquisition by reducing the mutagenic capacity in bacteria (Alam et al.,
394 2016). This indeed may be promising for treating certain bacteria, as demonstrated in *E. coli* (Alam et
395 al., 2016). However, our results show that for *A. baumannii*, inhibiting RecA may lead to robust biofilm
396 formation. It is thus important to understand the relationships between survival strategies in bacteria,
397 and that different bacteria may have different responses to treatment, based on their fundamental
398 biology. Overall, our results show the complex ways that *A. baumannii* robustly survives stress by
399 balancing alternative survival strategies through overlapping genetic pathways.

400

401 **Materials and Methods**

402 **Strains and Growth Conditions**

403 The strains and plasmids used are listed in Table S1. *A. baumannii* strains harboring the PNLAC1-*recA*
404 plasmid were constructed as before (Ching et al., 2017). The Δ*umuDAb* strain was constructed using

405 SOE PCR to insert a kanamycin gene cassette in the *umuDAb* gene as before (Norton et al., 2013). The
406 oligonucleotides used are in Table S1. All bacterial cultures were routinely grown in LB medium,
407 unless otherwise noted, and incubated at 37°C with shaking at 225 rpm for liquid cultures. YT medium
408 used is composed of 2.5-g NaCl, 10g Tryptone and 1g Yeast extract per liter. The solid medium
409 contained 1.5% agar (Fisher Bio-Reagents). Antibiotics were used at the following concentrations:
410 Kanamycin (Kan; 35 µg/mL), Gentamicin (Gm; 10 µg/mL), Tetracycline (Tet; 12 µg/mL), and
411 Carbenicillin (Carb; 100 µg/mL).

412

413 **Growth curve measurements**

414 Strains were diluted in the growth medium as indicated in the respective figure legends and grown in
415 YT medium in 96-well dishes. All strains were tested at least in triplicate. They were incubated in a
416 plate reader (Biotek Synergy H1) at 37ºC with shaking for 24 hrs with measurements of OD_{600} every
417 15 min.

418

419 **Pellicles & Colony Biofilm Formation**

420 To form pellicle biofilms, cells from a saturated culture were inoculated at a 1:1000 dilution into YT
421 liquid medium in either 6, 12 or 24-well non-tissue culture treated (lacking coating which change
422 surface properties) polystyrene plates. The same number of cells, adjusted based on optical density,
423 was added to each well. Plates were then incubated statically at 25°C. A standard Crystal violet staining
424 procedure was used to quantify adherence to the polystyrene surface (Chen et al., 2015). Early biofilms
425 are formed after 24 hrsh of static growth, and between 48-72 hrs. the biofilm has matured. After 72
426 hrs., the biofilms start to deteriorate. In the time course and gentamicin viable cell count experiments,

427 to correlate viable cells and biofilm formation, samples were taken for CFU counting from 3 wells per
428 experiment. The well content was thoroughly mixed before taking the samples, diluted with PBS, and
429 deposited on LB agar plates. After CFU sampling, the well content was aspirated, washed 3 times with
430 PBS, and stained with Crystal Violet as before (Ching et al., 2018). For colony biofilms, 3 µL of a
431 saturated bacterial culture were spotted on to YT agar plates containing 200µg/mL Congo red and
432 100µg/mL Coomassie brilliant blue (Congo red plates) (Ching et al., 2018) and incubated for 48 hrs.,
433 early colony biofilms, to 96 hrs. at 25°C. Images of biofilms were taken with a Leica MSV269
434 dissecting scope and a Leica DMC2900 camera, using the same settings. The radius of the biofilm
435 colonies was measured in triplicate from the dissecting microscope images at the same magnification.

436 For AB5075 colony, R2 medium with 1.5% agar (Reasoner and Geldreich, 1985) was used instead of
437 YT.

438 To prepare biofilms in which *recA* expression was knockdown by CRISPRi (Brychcy et al., n.d.), 0.5
439 % L-Arabinose was added to the YT medium to induce expression of the *dCas9* gene and inhition of
440 *recA* expression.

441

442 **Scanning Electron (SEM) and Transmission Electron (TEM) microscopy**

443 Biofilms for SEM were prepared by collecting pellicle biofilms on a glass coverslip treated with a
444 solution of 0.1 mg/mL of polylysine (Fisher Scientific). The coverslips with the biofilms were
445 deposited for at least 24 hrs. at 4ºC in wells with fixative 1 composed of 25% Glutaraldehyde, 0.1 M
446 Na-Cacodylate buffer (pH 7.2), 0.15% Alcian Blue and 0.15% Safranin. Additional treatment of the
447 coverslips and observation of the biofilms was performed at the Northeastern University Electron
448 Microscopy Core Facility.

449 For TEM, cultures were grown to saturation in YT liquid medium and streaked for single colonies on
450 YT plates incubated at 37°C. A colony was picked and gently resuspended in 100 µL of phosphate
451 buffered saline (PBS). 10 µL of the resuspended colony was pipetted onto a copper grid, excess liquid
452 wicked away with filter paper, and the grid was dried at room temperature. To negatively stain the
453 samples and observe pili, 10 µL of a solution of 1.5% phosphotungstic acid (PTA) was pipetted onto
454 the cell-containing grids. Liquid excess was wicked away with filter paper, and grids were left to air
455 dry at room temperature. Microscopy was performed with a JEOL JEM-1010 (JEOL USA, Peabody,
456 MA) microscope equipped with a 2k x 2k AMT CCD camera (Advanced Microscopy Techniques,
457 Woburn, MA) at the Northeastern University Electron Microscopy Core Facility.

458 **Sugar Extraction Assay**

459 The total extracellular matrix was extracted and total carbohydrate content was quantified using a
460 modified protocol from Jiao et al. 2010 (Jiao et al., 2010). Briefly, 500 µL of YT medium saturated
461 cultures of the *A. baumannii* strains were centrifuged at 13,000 rpm for 1 min in pre-weighed
462 microcentrifuge tubes and washed twice with 1X PBS; supernatant was discarded. Cell pellets were
463 dried at 95°C and reweighed. This process was repeated until all dried pellets were approximately equal
464 in weight (differences no more than 20% from each other). Pellets were reconstituted in 100 µL of 1X
465 PBS and 400 µL of a 0.1 M sulfuric acid solution was added to each tube. Cell suspensions were mixed
466 in a vortex every 10 minutes for 1 h.. Then, 250 µL of concentrated sulfuric acid (95% minimum) was
467 added, followed by 50 µL of freshly made 10% phenol solution in water. This mixture was incubated
468 at 95°C for 5 minutes. The absorbance at 492 nm of each sample was determined in a Biotek plate
469 reader (Synergy HT). This measurement represents the total carbohydrates. The absorbance per gram
470 of dry cell was normalized to the values obtained with the parental strain for each 3 biological
471 replicates. An unpaired two-tailed T-Test was used for statistical analysis relative to the parental strain:
472 * = $P<0.05$.

473

474 **Quantitative measurement of gene expression**

475 To measure *csu* transcripts in WT, Δ*recA*, and *recA*$^{++}$, we took 500µL of 24 hrs. saturated cells. These
476 were harvested by centrifugation and resuspended in 1 mL of RNA Protect Bacteria Reagent (Qiagen)
477 with 30µL of 20 mg/mL lysozyme, incubated at room temperature for 15 min, spun down at 15,000g
478 for 5 min, and cell pellets were stored at -20 ºC. Total RNA extraction was carried out by using the
479 Zymo Direct-zol RNA Kit (Zymo) according to manufacturer's instructions. A NanoDrop One
480 (ThermoFisher) was used to measure the RNA concentration and purity. RNA was converted to cDNA
481 using a high -capacity cDNA reverse transcription kit according to the manufacturer's protocol
482 (Applied Biosystems). Expression of *csuAB* pili gene expression by RT-qPCR was performed with
483 cDNA using the qPCR primer pairs listed in Table S1 and following the protocol for Fast SYBR Green
484 Master Mix (Applied Biosystems) using a StepOnePlus real-time PCR instrument (Applied
485 Biosystems). The relative gene expression was standardized using endogenous 16S ribosomal RNA
486 expression, and the comparative threshold cycle (ΔΔCT) was calculated for each sample and compared
487 relative to WT expression. Each sample was run in biological and technical triplicates. An unpaired
488 two -tail T test was used for statistical analysis relative to the parental strain (*=$P < 0.05$).

489

490 **Pilus purification.**

491 Pilus shear preparations were performed as previously published (Moon et al., 2017). Briefly, a similar
492 number of cells grown on a YT agar plate (OD_{600}~20) were collected in 1.5 mL of 1X PBS, placed on
493 ice for 10 min, and vortexed for 1 min. After centrifugation at 13,000 x g at 4ºC, cell supernatants
494 (containing the pili) and the respective pellets (containing pili-less cells) were collected. The pili within

495 the supernatants were precipitated for 20 h with trichloroacetic acid (TCA) (final concentration, 25%),
496 at -20°C. The precipitated pili were collected by centrifugation at 16,000 x g for 10 min at 4°C and
497 resuspended in 50 µL 1X PBS. Total protein was extracted from pili-free cell pellets and whole cell
498 lysates using Bugbuster reagent (Novagen) following the manufacturer's instructions and quantified
499 using a Bradford assay.

500

501 **Purification of His-tagged *A. baumannii* RecA and Immunoblots**

502 The *recA* gene from *A. baumannii* was amplified using the primers RecALICF and RecALICR (Table
503 S1), ligated into the pET-His6-TEV-LIC vector (plasmid 29653; Addgene, Cambridge, MA, USA)
504 using the Ligation Independent Cloning Protocol (Gradia et al., 2017), and introduced by
505 transformation into DH5α *E. coli* cells for plasmid maintenance. The induction of expression and
506 purification methods are as previously described for RecA purification from *E. coli* (Tashjian et al.,
507 2017). RecA purification was confirmed by SDS-PAGE.

508

509 For the semi-quantitative western blots, saturated cultures were diluted 1:100 and grown to an
510 exponential phase. Cells were then treated with ciprofloxacin (Cip) at 10X the MIC for 3 h. (Ching et
511 al., 2017). A parallel culture for each strain was left untreated. Cells were collected by centrifugation,
512 and whole-protein lysate was extracted using Bugbuster reagent (Novagen) and Pierce Universal
513 Nuclease according to manufacturer's instructions. Cell -free lysates were quantified with a Bradford
514 assay following the manufacturer's instructions (BioRad). Lysate was diluted to 1X with Laemmli
515 buffer and heated for 10 min at 95ºC. The samples were separated on a 12% Bis-Tris gel (Invitrogen)
516 in MOPS buffer and transferred to a nitrocellulose membrane (Cafarelli et al., 2013). The blot was
517 developed as before (Cafarelli et al., 2013) using a primary anti-RecA antibody (Abcam) at a 1:10,000

518 dilution (Norton et al., 2013) and an HRP-labelled secondary goat anti-rabbit antibody (Abcam) diluted
519 at 1:40,000. Image J was used to quantify the density of the RecA bands (Norton et al., 2013). The
520 RecA signal from all samples were compared to a standard of purified RecA protein from *A.*
521 *baumannii*. Cmmassie Blue staining was used to estimate similar loading of lanes of a parallel gel. The
522 procedure was done in 4 biological replicates. RecA determinations were similar every time.
523

524 To measure the relative amount of Csu pili in the different strains, we performed immunoblots with an
525 anti-Csu antibody (gracious gift from Luis Actis). The pili content of each strain was standardized to
526 the total protein measured in the cell-free extracts from which the pili were isolated. To detect Csu pili
527 from whole cell lysates, a similar number of cells were lysed with Bugbuster and Pierce Universal
528 Nuclease as indicated above. The samples were separated in a 12% polyacrylamide gel in MES buffer
529 at 150V for 1 h.. Immunoblot procedures were followed as described above using a 1:1000 dilution of
530 the anti-Csu primary antiserum and a 1:40,000 dilution of the HRP labeled secondary anti-rabbit
531 antibody (Abcam). A ChemiDoc MP imaging system (BioRad) was used for chemiluminescence signal
532 detection from RecA and Csu blots.

533

534 **EMSA for UmuDAb to the promoter of *bfmR***

535 The full-length *umuDAb* and truncated *umuDAb* (*umuD'Ab,* C-terminal end based on previously
536 determined cleavage site (Hare et al., 2013)) genes were tagged with a hexahistidine tag on the C-
537 terminal end and cloned into pET11T (Nguyen et al., 1993). The constructs were introduced into BL21
538 AI cells and His-UmuDAb and His-UmuD'Ab were overexpressed as previously described (Cafarelli
539 et al., 2013; Studier, 2005). Both proteins were then purified by immobilized metal affinity
540 chromatography as described previously (Cafarelli et al., 2014).

541

542 PCR amplification with primers (bfmR_umuD_motif_F(Cy3) and bfmR_umuD_motif_R, Table S1)
543 labeled with a Cy3 fluorophore on the 5' end was used to create the *bfmR* DNA probe. DNA (25 nM)
544 and protein were mixed with binding buffer (10mM Tris-HCl [pH 8], 10mM HEPES, 50mM KCl,
545 1mM EDTA, 100 ng of salmon sperm DNA, 0.1 mg of bovine serum albumin per ml). Binding
546 reactions were incubated for one h at 37°C. Reaction mixtures (20 ul) were loaded into a 5%
547 nondenaturing Tris-borate-EDTA (TBE) polyacrylamide gel. Binding complexes were separated at
548 150V for one hour. Cy3-labelled DNA-protein complexes were visualized using a Bio-rad Chemidoc
549 imager. All the EMSAs were repeated thrice.

550

551 **Construction of the P$_{csu}$-*gfp*, P$_{csuAB}$-*mCherry* and P*bfmr-mkate2* expression reporter plasmids and**
552 **expression assays**

553 *A. baumannii* ATCC 17978 containing a *csu* operon (P$_{csuAB}$-*gfp*) transcriptional reporter on the
554 Carbenicillin (Carb) resistant plasmid pMB1-A(Brychcy et al., n.d.), a modified version of the EcoFlex
555 kit (Moore et al., 2016) containing replication elements necessary for *A. baumannii*, was used to assess
556 the expression of Csu in the WT, *recA*$^{++}$, and Δ*recA* strains. The promoter region of the *csu* operon and
557 of *bfmr* were amplified using the primers csu_f and csu_r, and pBfmR_f and pBfmR_r respectively.
558 The plasmid pBP_lacZ (Table S1; Addgene accession number 72948) and the purified PCR fragment
559 were digested using SphI and NdeI, and the pBP-lacZ plasmid was dephosphorylated using QuickCIP
560 (all enzymes from NEB). The ligation was carried out with T4 DNA ligase (Thermo Fisher Scientific).
561 Colonies were screened using blue-white color in plates with X-Gal and verified by colony PCR and
562 sequencing using Primers pBP_pTU_f and pBP_r. This generated level 0 MoClo plasmids for the
563 promoter elements.

564

565 Plasmids with the desired inserts were then used in a combined cloning and ligation reaction, by using
566 20 fmol of each entry vector (pBP_*pcsu* or pBP_*pbfmr*, pBP_B0012, pBP_e*gfp;* pBP_*mcherry* or
567 pBP_*mkate2*, pBP_pET-RBS and pTU1-A-RFP-AB) combined with 2 µL of Cutsmart, 0.5 µL of BsaI-
568 HFv2, 0.5 µL of T4 DNA Ligase and 1 µL of 10 mM ATP (all reagents from New England Biolabs,
569 Ipswich, MA., except T4 DNA Ligase from Thermo Fisher Scientific). The reaction was cycled 50
570 times in a thermocycler with a 37 °C digestion step for 2 minutes and a 16 °C ligation step for 5
571 minutes. Plasmids with no insert were eliminated by digestion with BsaI at 37 °C for 1 h. The enzymes
572 were heat-inactivated at 80°C for 10 min. 5 µL of the ligation mix was introduced by transformation
573 into chemically competent *E. coli* DH5α. White colonies contain the desired insert due to the exchange
574 of the mCherry gene originally in the pMB1-A cloning site and confirmed by colony PCR and
575 sequencing the insert using pBP_pTU_f and pTU_r. Plasmids were introduced by transformation into
576 *A. baumannii* using standard electroporation protocols (MacGuire et al., 2014).

577

578 To quantify fluorescence in single cells, at least 300 single cells were counted, and their fluorescence
579 was measured with MicrobeJ from microscope images taken with the same settings(Ducret et al.,
580 2016).

581

582 **Construction of *recA* knockdown CRISPRi plasmids**

583 CRISPRi constructs were created according to Brychcy et al.(Brychcy et al., n.d.). Briefly, 5 uL of
584 100uM of each sgRNA oligonucleotide (recA_ORF_sgRNA_f and recA_ORF_sgRNA_r or
585 nonsense_sgRNA_f and nonsense_sgRNA_r) were annealed in T4 DNA ligase buffer by incubating at
586 95 °C for 5 minutes and subsequent cooling to 22 °C for 20 minutes. 1 uL of the annealed
587 oligonucleotides was then used in a Golden Gate reaction as described above, using BpiI-HF (NEB) as

588 restriction and pBP_sgRNA (Addgene number: 190128) as the target vector, generating the level 0
589 plasmid pBP_recA_sgRNA or pBP_nonsense_sgRNA respectively. Subsequently, this plasmid was
590 used in a Golden Gate reaction using pMB1-B (Addgene number 190115) and BsaI-HF (NEB) as
591 restriction enzyme, generating pMB1-B-recA_sgRNA. Lastly, pMB1-B-recA was recombined with
592 pMB1-A-pBAD-dCas9 (Addgene number: 190132) in the target plasmid pMB2a-tet (a modified
593 version of Addgene number: 190120 containing TetR instead of KanR) generating the plasmid pMB2a-
594 pBAD_dCas-recA_sgRNA and pMB2a-pBAD_dCas9-nonsense_sgRNA. The plasmids were
595 confirmed via sequencing with the oligonucleotides mentioned in the chapter above. Both plasmids
596 were subsequently transformed into A. baumannii ATCC17978 WT, *ΔrecA*, *ΔumuDAB*, *ΔcsuD* (Moon
597 et al., 2017)(kindly provided by Mario Feldman), and *Δbfmr* (EGA496, kindly provided by Edward
598 Geisinger, Northeastern University) via electroporation.
599

600 **Microscopy and GFP reporter measurements**

601 To perform confocal microscopy experiments, we used a Zeiss Axio Observer. Z1/7. The
602 excitation/emission used were 280/618 nm for the red channel, and 488/509 nm for the green channel.
603 We formed biofilms in wells, and after 48 h, 0.5xMIC Cip was added underneath the pellicles and
604 dishes were incubated statically for an additional 48 hrs. Pellicles were collected from mock -treated
605 and Cip-treated wells on a glass coverslip treated with 0.1 mg/mL of polylysine to facilitate attachment.
606 The side of the pellicle in direct contact with the liquid medium was in contact with the glass, and the
607 side of the biofilm in contact with air remained as such. Z-stacks were of 1µm.
608

609 For the GFP reporter measurements, GFP fluorescence was measured in a plate reader (Biotek synergy
610 H1) for at least 24 h. at 25ºC without shaking. To start the experiment, cultures were diluted 1:100 in
611 YT medium in a 96 multi-well dish. Green fluorescence (Excitation 479 nm and emission 520 nm) and

612 OD_{600} were measured every 15 min. Growth and fluorescence data were gathered at least in triplicate
613 for each strain.
614

615 **MIC and Biofilm Eradication Assays, and Live/Dead determination.**

616 Standard assays were used to test for MIC (Andrews, 2001) in planktonic shaking cultures. Pellicles
617 were set up as described above and incubated statically at 25°C for the number of hours indicated in
618 the respective figure legends, at which time free cells (not in biofilms) were removed, and wells washed
619 thrice with 1X PBS. YT medium containing Gm, at a range of concentrations shown in the respective
620 figures was added to each washed well. The plate was then incubated statically for 24 hrs. at 25°C,
621 after which the spent medium was removed, and wells were washed three times with PBS. Crystal
622 Violet staining was then carried out as before (Chen et al., 2015). Plating for viable counts was
623 performed as described earlier.

624

625 **Competing Interests**

626 The authors declare no competing interests.

627 **Acknowledgments**

628 We would like to acknowledge the members of the Godoy, Chai, and Geisinger labs at Northeastern
629 University for helpful comments and discussion. We would like to thank G. Bou from Servicio de
630 Microbiologia, Complejo Hospitalario Universitario, La Coruña, Spain for the Δ*recA* strain, Luis Actis
631 from the Department of Microbiology, Miami University, for the anti-Csu antibody, Stephen Lory from
632 Harvard Medical School for access to the AB7505 transposon collection, Mario Feldman from
633 Washington University St. Louis Medical School for the for Δ*csuD* strain and Edward Geisinger from

634 the Department of Biology, Northeastern University for the Δ*bfmR* strain (EGA496). M.D. and S.R.
635 were funded by the Undergraduate Research and Fellowships office at Northeastern University. V.G.G
636 used funding from a stipend from NUSci, an Inclusive Excellence award form HHMI, Y.C. from an
637 NSF grant (MCB1651732), and A.R. by a Northeastern University Provost Dissertation Completion
638 Fellowship.

639

640 **Author Contributions**

641 V.G.G., and C.C. initiated research in discussions with YC. B. I. performed preliminary experiments.
642 C.C., P.M., A.R., M. B., B. N., S. R., M.D., W. F., and V.G.G. performed experiments and analyzed
643 data. C.C. and V.G.G. wrote the manuscript.

644

645

646

647

648

649

650

651

652

653

654

655

656

657 **References:**

658 Alam K, Alhhazmi A, Decoteau JF, Luo Y, Geyer CR, Alam K, Alhhazmi A, Decoteau JF, Luo Y,
659 Geyer CR. 2016. RecA Inhibitors Potentiate Antibiotic Activity and Block Evolution of
660 Antibiotic Resistance Article RecA Inhibitors Potentiate Antibiotic Activity and Block
661 Evolution of Antibiotic Resistance. *Cell Chem Biol* **23**:381–391.
662 doi:10.1016/j.chembiol.2016.02.010
663 Anderl JN, Franklin MJ. 2000. Role of Antibiotic Penetration Limitation in Klebsiella pneumoniae
664 Biofilm Resistance to Ampicillin and Ciprofloxacin. *Antimicrob Agents Chemother* **44**:1818–
665 1824.
666 Andrews JM. 2001. Determination of minimum inhibitory concentrations. *Journal of Antimicrobial*
667 *Chemotherapy* 5–16.
668 Aranda J, Bardina C, Beceiro A, Rumbo S, Cabral MP, Barbé J, Bou G. 2011. Acinetobacter
669 baumannii RecA protein in repair of DNA damage, antimicrobial resistance, general stress
670 response, and virulence. *J Bacteriol* **193**:3740–7. doi:10.1128/JB.00389-11
671 Asally M, Kittisopikul M, Rue P, Du Y, Hu Z, Cagatay T, Robinson AB, Lu H, Garcia-Ojalvo J, Suel
672 GM. 2012. Localized cell death focuses mechanical forces during 3D patterning in a biofilm.
673 *Proceedings of the National Academy of Sciences* **109**:18891–18896.
674 doi:10.1073/pnas.1212429109
675 Bales PM, Renke EM, May SL, Shen Y, Nelson DC. 2013. Purification and Characterization of
676 Biofilm-Associated EPS Exopolysaccharides from ESKAPE Organisms and Other Pathogens.
677 *PLoS One* **8**. doi:10.1371/journal.pone.0067950
678 Blair JMA, Webber MA, Baylay AJ, Ogbolu DO, Piddock LJ v. 2014. Molecular mechanisms of
679 antibiotic resistance. *Nat Rev Microbiol* **13**:42–51. doi:10.1038/nrmicro3380
680 Brossard KA, Campagnari AA. 2012. The Acinetobacter baumannii Biofilm-Associated Protein
681 Plays a Role in Adherence to Human Epithelial Cells. *Infect Immun* 228–233.
682 doi:10.1128/IAI.05913-11
683 Brychcy M, Kokodynski A, Lloyd D, Godoy VG. n.d. AspFlex: molecular tools to study gene
684 expression and regulation in. *bioRxiv*. doi:10.1101/2023.03.17.533205
685 Cafarelli TM, Rands TJ, Benson RW, Rudnicki PA, Lin I, Godoy VG. 2013. A single residue unique
686 to dinb-like proteins limits formation of the polymerase IV multiprotein complex in Escherichia
687 coli. *J Bacteriol* **195**:1179–1193. doi:10.1128/JB.01349-12
688 Cafarelli TM, Rands TJ, Godoy VG. 2014. The DinB.RecA Complex of Escherichia coli Mediates an
689 Efficient and High-Fidelity Response to Ubiquitous Alkylation Lesions. *Mutat Res Genet*
690 *Toxicol Environ Mutagen* **51**:229–235. doi:10.1002/em
691 Chen Y, Gozzi K, Yan F, Chai Y. 2015. Acetic acid acts as a volatile signal to stimulate bacterial
692 biofilm formation. *mBio* **6**:1–13. doi:10.1128/mBio.00392-15
693 Ching C, Gozzi K, Heinemann B, Chai Y, Godoy VG. 2017. RNA-Mediated cis Regulation in
694 Acinetobacter baumannii Modulates Stress-Induced Phenotypic Variation. *J Bacteriol* **199**:1–15.
695 Ching C, Yang B, Onwubueke C, Lazinski D, Camilli A, Godoy VG. 2018. Lon protease has
696 multifaceted biological functions in *Acinetobacter baumannii*. *J Bacteriol* **201**:1–12.
697 doi:10.1128/JB.00536-18
698 Choi AH, Slamti L, Avci FY, Pier GB. 2009. The pgaABCD Locus of Acinetobacter baumannii
699 Encodes the Production of Poly- ᴺ -1-6- N -Acetylglucosamine , Which Is Critical for Biofilm
700 Formation . *J Bacteriol* **191**:5953–5963. doi:10.1128/JB.00647-09
701 Cirz RT, Jones MB, Gingles NA, Minogue TD, Jarrahi B, Peterson SN, Romesberg FE. 2007.
702 Complete and SOS-mediated response of Staphylococcus aureus to the Antibiotic
703 Ciprofloxacin. *J Bacteriol* **189**:531–539. doi:10.1128/JB.01464-06

704 Costa SB, Campos ACC, Pereira ACM, de Mattos-Guaraldi AL, Junior RH, Rosa ACP, Asad
705 LMBO. 2014. Adherence to abiotic surface induces SOS response in Escherichia coli K-12
706 strains under aerobic and anaerobic conditions. *Microbiology (N Y)* **160**:1964–1973.
707 doi:10.1099/mic.0.075317-0
708 Costerton JW, Lewandowski Z, Caldwell DE, Korber DR, Sn S, Lappin-scott HM. 1995. Microbial
709 biofilms. *Annu Rev Microbiol* 711–745.
710 Cox JM, Li H, Wood EA, Chitteni-Pattu S, Inman RB, Cox MM. 2008. Defective dissociation of a
711 "slow" RecA mutant protein imparts an Escherichia coli growth defect. *Journal of Biological*
712 *Chemistry* **283**:24909–24921. doi:10.1074/jbc.M803934200
713 Draughn GL, Milton ME, Feldmann EA, Bobay BG, Roth BM, Olson AL, Thompson RJ, Actis LA,
714 Davies C, Cavanagh J. 2018. The Structure of the Biofilm-controlling Response Regulator
715 BfmR from Acinetobacter baumannii Reveals Details of Its DNA-binding Mechanism. *J Mol*
716 *Biol* **430**:806–821. doi:10.1016/j.jmb.2018.02.002
717 Ducret A, Quardokus E, Brun Y. 2016. MicrobeJ, a high throughput tool for quantitative bacterial
718 cell detection and analysis. *Nature Microbiol* **1**:1–7. doi:10.1038/nmicrobiol.2016.77
719 Erlandsen SL, Kristich CJ, Dunny GM, Wells CL. 2004. High-resolution Visualization of the
720 Microbial Glycocalyx with Low-voltage Scanning Electron Microscopy : Dependence on
721 Cationic Dyes The Journal of Histochemistry & Cytochemistry. *Journal of Histochemistry and*
722 *Cytochemistry* **52**:1427–1435. doi:10.1369/jhc.4A6428.2004
723 Eze EC, Chenia HY, el Zowalaty ME. 2018. Acinetobacter baumannii biofilms : effects of
724 physicochemical factors , virulence , antibiotic resistance determinants , gene regulation , and
725 future antimicrobial treatments. *Infect Drug Resist* **11**:2277–2299.
726 Farrow JM, Wells G, Pesci EC. 2018. Desiccation tolerance in Acinetobacter baumannii is mediated
727 by the two-component response regulator BfmR. *PLoS One* **13**:1–25.
728 doi:10.1371/journal.pone.0205638
729 Fuchs RP, Fujii S. 2013. Translesion DNA Synthesis and Mutagenesis in Prokaryotes. *Cold Spring*
730 *Harb Perspect Biol* 1–22.
731 Gaddy JA, Actis LA. 2009. Regulation of Acinetobacter baumannii biofilm formation. *Future*
732 *Microbiol* **4**:273–278. doi:10.2217/fmb.09.5.Regulation
733 Gallagher LA, Ramage E, Weiss EJ, Radey M, Hayden HS, Held KG, Huse HK, Zurawski D v.,
734 Brittnacher MJ, Manoil C. 2015. Resources for genetic and genomic analysis of emerging
735 pathogen Acinetobacter baumannii. *J Bacteriol* **197**:2027–2035. doi:10.1128/JB.00131-15
736 Geisinger E, Isberg RR. 2015. Antibiotic Modulation of Capsular Exopolysaccharide and Virulence
737 in Acinetobacter baumannii. *PLoS Pathog* **11**:1–27. doi:10.1371/journal.ppat.1004691
738 Ghodke H, Paudel BP, Lewis JS, Jergic S, Gopal K, Romero ZJ, Wood EA, Woodgate R, Cox MM,
739 Oijen AMV. 2019. Spatial and temporal organization of reca in the escherichia coli dna-damage
740 response. *Elife* **8**:1–37. doi:10.7554/eLife.42761
741 Gozzi K, Ching C, Paruthiyil S, Zhao Y, Godoy VG, Chai Y. 2017. Bacillus subtilis utilizes the DNA
742 damage response to manage multicellular development. *NPJ Biofilms Microbiomes* **3**:8.
743 doi:10.1038/s41522-017-0016-3
744 Gradia S, Ishida JP, Tsai M, Jeans C, Tainer JA, States U, Bioimaging I, Berkeley L, States U,
745 Berkeley L, States U, States U, States U. 2017. MacroBac: New technologies for robust and
746 efficient large-scale production of recombinant multi-protein complexes. *Methods Enzymol*.
747 doi:10.1016/bs.mie.2017.03.008.MacroBac
748 Hardouin J, Chabane YN, Marti S, Rihouey C. 2014. Characterisation of Pellicles Formed by
749 Acinetobacter baumannii at the Air-Liquid Interface. *PLoS One* **9**.
750 doi:10.1371/journal.pone.0111660

751 Hare JM, Adhikari S, Lambert K V, Hare AE, Alison N. 2013. The Acinetobacter regulatory
752 UmuDAb protein cleaves in response to DNA damage with chimeric LexA/UmuD
753 characteristics. *FEMS Microbiol Lett* **334**:57–65. doi:10.1111/j.1574-6968.2012.02618.x.The
754 Hare JM, Ferrell JC, Witkowski T a, Grice AN. 2014. Prophage induction and differential RecA and
755 UmuDAb transcriptome regulation in the DNA damage responses of Acinetobacter baumannii
756 and Acinetobacter baylyi. *PLoS One* **9**:e93861. doi:10.1371/journal.pone.0093861
757 He X, Lu F, Yuan F, Jiang D, Zhao P, Zhu J, Chene H, Cao J, Lu G. 2015. Biofilm Formation
758 Caused by Clinical Acinetobacter baumannii Isolates Is Associated with Overexpression of the
759 AdeFGH Efflux Pump. *Antimicrob Agents Chemother* **59**:4817–4825. doi:10.1128/AAC.00877-
760 15
761 Inagaki S, Fujita K, Nagayama K, Funao J, Effects OT. 2009. Effects of recombinase A deficiency
762 on biofilm formation by Streptococcus mutans. *Oral Microbiol Immunol* 104–108.
763 Jacobs AC, Thompson MG, Black CC. 2014. AB5075 , a Highly Virulent Isolate of Acinetobacter
764 baumannii , as a. *mBio* **5**:1–10. doi:10.1128/mBio.01076-14.Editor
765 Jiao Y, Cody GD, Harding AK, Wilmes P, Schrenk M, Wheeler KE, Banfield JF, Thelen MP,
766 Carolina N. 2010. Characterization of Extracellular Polymeric Substances from Acidophilic
767 Microbial Biofilms □ †. *Appl Environ Microbiol* **76**:2916–2922. doi:10.1128/AEM.02289-09
768 Kreuzer KN. 2013. DNA Damage Responses in Prokaryotes: Regulating Gene Expression,
769 Modulating Growth Patterns, and Manipulating Replication Forks. *Cold Spring Harb Perspect*
770 *Biol* 1–23.
771 Linares JF, Gustafsson I, Baquero F, Martinez JL. 2006. Antibiotics as intermicrobial signaling
772 agents instead of weapons. *Proc Natl Acad Sci U S A* **103**:19484–19489.
773 doi:10.1073/pnas.0608949103
774 Little JW, Mount DW. 1982. The SOS Regulatory Escherichia coli System of Review **29**:1982.
775 Loehfelm TW, Luke NR, Campagnari AA. 2008. Identification and characterization of an
776 Acinetobacter baumannii biofilm-associated protein. *J Bacteriol* **190**:1036–1044.
777 doi:10.1128/JB.01416-07
778 Luke NR, Sauberan SL, Russo TA, Beanan JM, Olson R, Loehfelm TW, Cox AD, Michael FS,
779 Vinogradov E v, Campagnari AA. 2010. Identification and Characterization of a
780 Glycosyltransferase Involved in Acinetobacter baumannii Lipopolysaccharide Core
781 Biosynthesis □. *Infect Immun* **78**:2017–2023. doi:10.1128/IAI.00016-10
782 MacGuire AE, Ching MC, Diamond BH, Kazakov A, Novichkov P, Godoy VG. 2014. Activation of
783 phenotypic subpopulations in response to ciprofloxacin treatment in Acinetobacter baumannii.
784 *Mol Microbiol* **92**:138–52. doi:10.1111/mmi.12541
785 Moon KH, Weber BS, Feldman F. 2017. Subinhibitory Concentrations of Trimethoprim and
786 Sulfamethoxazole Acinetobacter baumannii through Inhibition of Csu Pilus Expression.
787 *Antimicrob Agents Chemother* **61**:1–18.
788 Moore SJ, Lai HE, Kelwick RJR, Chee SM, Bell DJ, Polizzi KM, Freemont PS. 2016. EcoFlex: A
789 Multifunctional MoClo Kit for E. coli Synthetic Biology. *ACS Synth Biol* **5**:1059–1069.
790 doi:10.1021/acssynbio.6b00031
791 Nguyen LH, Jensen DB, Burgess RR. 1993. Overproduction and purification of σ32, the Escherichia
792 coli heat shock transcription factor. *Protein Expr Purif* **4**:425–433.
793 Norton MD, Spilkia AJ, Godoy VG. 2013. Antibiotic Resistance Acquired through a DNA Damage-
794 Inducible Response in Acinetobacter baumannii. *J Bacteriol* **195**:1335–45.
795 doi:10.1128/JB.02176-12
796 Pakharukova N, Tuittila M, Paavilainen S, Malmi H, Parilova O, Teneberg S, Knight SD, Zavialov A
797 v. 2018. Structural basis for Acinetobacter baumannii biofilm formation. *Proc Natl Acad Sci U*
798 *S A* **115**:5558–5563. doi:10.1073/pnas.1800961115

799 Peleg AY, Seifert H, Paterson DL. 2008. Acinetobacter baumannii: Emergence of a successful
800 pathogen. *Clin Microbiol Rev* **21**:538–582. doi:10.1128/CMR.00058-07
801 Reasoner DJ, Geldreich EE. 1985. A new medium for the enumeration and subculture of bacteria
802 from potable water. *Appl Environ Microbiol* **49**:1–7. doi:10.1128/aem.49.1.1-7.1985
803 Rice LB. 2008. Federal Funding for the Study of Antimicrobial Resistance in Nosocomial
804 Pathogens : No ESKAPE. *J Infect Dis* **197**:1079–1081. doi:10.1086/533452
805 Rumbo-Feal S, Gómez MJ, Gayoso C, Álvarez-Fraga L, Cabral MP, Aransay AM, Rodríguez-
806 Ezpeleta N, Fullaondo A, Valle J, Tomás M, Bou G, Poza M. 2013. Whole Transcriptome
807 Analysis of Acinetobacter baumannii Assessed by RNA-Sequencing Reveals Different mRNA
808 Expression Profiles in Biofilm Compared to Planktonic Cells. *PLoS One* **8**:1–19.
809 doi:10.1371/journal.pone.0072968
810 Russo TA, Manohar A, Beanan JM, Olson R, MacDonald U, Graham J, Umland TC. 2016. The
811 Response Regulator BfmR Is a Potential Drug Target for Acinetobacter baumannii . *mSphere*
812 **1**:1–19. doi:10.1128/msphere.00082-16
813 Sahu PK, Iyer PS, Oak AM, Pardesi KR, Chopade BA. 2012. Characterization of eDNA from the
814 Clinical Strain Acinetobacter baumannii AIIMS 7 and Its Role in Biofilm Formation. *The*
815 *Scientific World Journal* **2012**. doi:10.1100/2012/973436
816 Santos-Lopez A, Marshall CW, Scribner MR, Snyder DJ, Cooper VS. 2019. Evolutionary pathways
817 to antibiotic resistance are dependent upon environmental structure and bacterial lifestyle. *Elife*
818 **8**:1–23. doi:10.7554/elife.47612
819 Shaner NC, Steinbach PA, Tsien RY. 2005. A guide to choosing fluorescent proteins. *Nat Methods*
820 **2**:905–909. doi:10.1038/nmeth819
821 Singh R, Sahore S, Kaur P, Rani A, Ray P. 2016. Penetration barrier contributes to bacterial biofilm-
822 associated resistance against only select antibiotics , and exhibits genus- , strain- and antibiotic-
823 specific differences. *Pathog Dis* 2–7. doi:10.1093/femspd/ftw056
824 Smith MG, Gianoulis T a, Pukatzki S, Mekalanos JJ, Ornston LN, Gerstein M, Snyder M. 2007. New
825 insights into Acinetobacter baumannii pathogenesis revealed by high-density pyrosequencing
826 and transposon mutagenesis. *Genes Dev* **21**:601–14. doi:10.1101/gad.1510307
827 Studier FW. 2005. Protein production by auto-induction in high density shaking cultures. *Protein*
828 *Expr Purif* **41**:207–234. doi:10.1016/j.pep.2005.01.016
829 Surgalla MJ, Beesley ED. 1969. Congo red-agar plating medium for detecting pigmentation in
830 Pasteurella pestis. *Appl Microbiol* **18**:834–837.
831 Takajashi A, Yomoda S, Ushijima I, Inoue M. 1995. Orfloxacin, norfloxacin and ceftazimide
832 increase the production of alginate and promote the formation of biofilm of Pseudomonase
833 aeruginosa in vitro. *Journal of Antimicrobial Chemotherapy*.
834 Tashjian TF, Lin I, Belt V, Cafarelli TM, Godoy VG. 2017. RNA primer extension hinders DNA
835 synthesis by Escherichia coli mutagenic DNA polymerase IV. *Front Microbiol* **8**:1–9.
836 doi:10.3389/fmicb.2017.00288
837 Tomaras AP, Dorsey CW, Edelmann RE, Actis LA. 2003. Attachment to and biofilm formation on
838 abiotic surfaces by Acinetobacter baumannii: Involvement of a novel chaperone-usher pili
839 assembly system. *Microbiology (N Y)* **149**:3473–3484. doi:10.1099/mic.0.26541-0
840 Tomaras AP, Flagler MJ, Dorsey CW, Gaddy JA, Actis LA. 2008. Characterization of a two-
841 component regulatory system from Acinetobacter baumannii that controls biofilm formation and
842 cellular morphology. *Microbiology (N Y)* **154**:3398–3409. doi:10.1099/mic.0.2008/019471-0
843 Vlamakis H, Chai Y, Beauregard P, Losick R, Kolter R. 2013. Sticking together: Building a biofilm
844 the Bacillus subtilis way. *Nat Rev Microbiol* **11**:157–168. doi:10.1038/nrmicro2960
845 Walter BM, Cartman ST, Minton NP, Butala M, Rupnik M, B.M. W, S.T. C, N.P. M, M. B, M. R,
846 Walter BM, Cartman ST, Minton NP, Butala M, Rupnik M. 2015. The SOS Response Master

847 Regulator LexA Is Associated with Sporulation, Motility and Biofilm Formation in Clostridium
848 difficile. *PLoS One* **10**:e0144763–e0144763. doi:10.1371/journal.pone.0144763
849 Wang Y, Huang T, Yang Y, Kuo S, Chen C. 2018. Biofilm formation is not associated with worse
850 outcome in Acinetobacter baumannii bacteraemic pneumonia. *Sci Rep* 1–10.
851 doi:10.1038/s41598-018-25661-9
852 Werner E, Roe F, Bugnicourt A, Franklin MJ, Heydorn A, Molin S, Pitts B, Stewart PS. 2004.
853 Stratified Growth in Pseudomonas aeruginosa Biofilms. *Appl Environ Microbiol* **70**:6188–6196.
854 doi:10.1128/AEM.70.10.6188
855 Witkowski TA, Grice AN, Stinnett DB, Wells WK, Peterson MA, Hare JM. 2016. UmuDAb : An
856 Error-Prone Polymerase Accessory Homolog Whose N-Terminal Domain Is Required for
857 Repression of DNA Damage Inducible Gene Expression in Acinetobacter baylyi. *PLoS One* 1–
858 19. doi:10.1371/journal.pone.0152013
859
860
861
862
863
864
865
866
867
868
869
870
871
872
873
874
875
876
877
878

879 **Figures And Figure Legends**

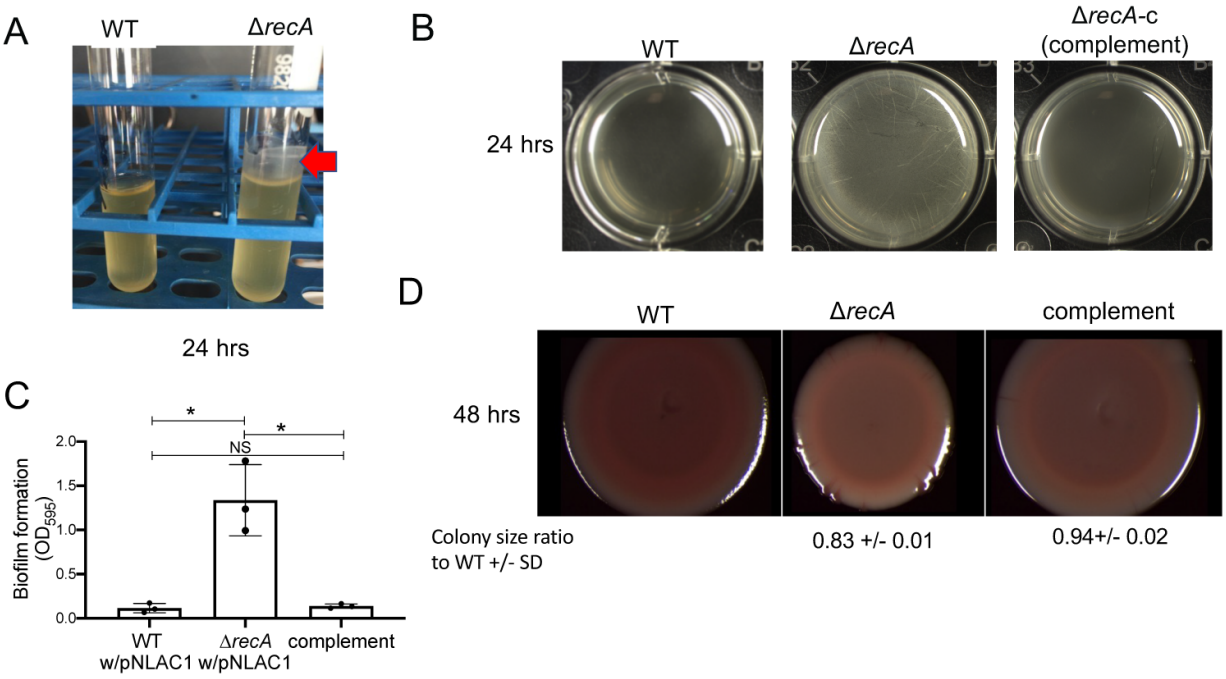

880

881 **Figure 1. RecA negatively influences surface attachment and biofilm formation. (A)** Saturated
882 Δ*recA* cell cultures show visible growth on the side surface of glass test tubes (red arrow) compared to
883 WT cells. (**B)** Δ*recA* forms visible pellicles biofilms at the air-liquid interface earlier than its isogenic
884 WT counterpart. Biofilm pellicles of WT (with empty PNLAC1 plasmid), Δ*recA* (with empty PNLAC1
885 plasmid), and the complemented strain (Δ*recA*(pNLAC1-*recA,* Δ*recA*-c) at 24 hrs. Representative
886 images are shown. (**C)** Δ*recA* cells adhere to the abiotic surface better than WT and the Δ*recA*-c strain.
887 Graph shows absorbance at 595 nm for Crystal Violet staining of polystyrene surface-adhered cells at
888 24 hrs. Experiments were performed in triplicate and error bars shown represent standard deviation of
889 the mean. An unpaired two-tailed T-test was performed for statistical analysis, * =P < 0.05, NS=not
890 significant. Brackets above the columns indicate the comparisons made. (**D**) RecA influences colony
891 biofilm architecture and coloration. Colony biofilms of WT, Δ*recA*, and Δ*recA*-c strains on Congo Red
892 plates at 48 hrs. Numbers underneath the images represent the average diameter of 3 colonies from
893 images taken at the same magnification and settings in 3 independent experiments relative to the WT
894 colony diameter set as 1. The error represents the standard deviation of the mean.

895

896

897

898

899

900

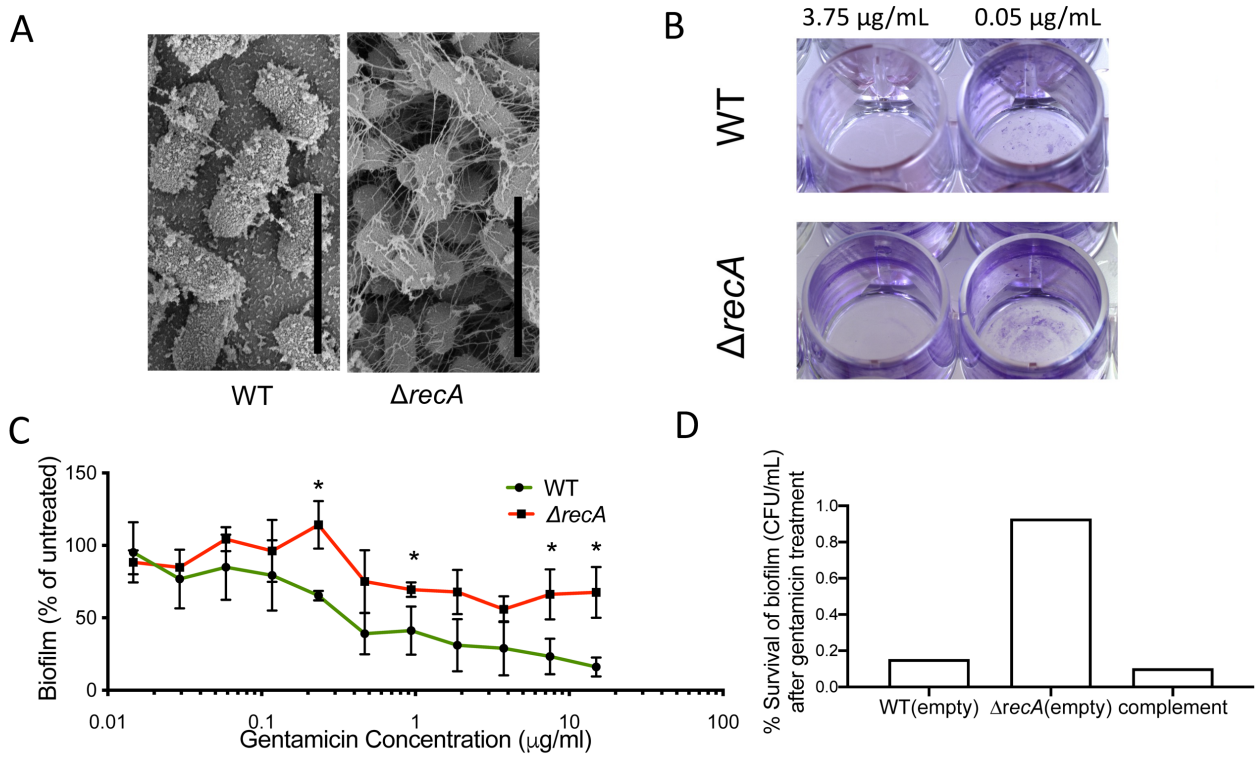

Figure 2. Biofilm formation influences antibiotic challenge (**A**) Δ*recA* biofilms have increased observable matrix compared to WT biofilms. Scanning electron microscopy (SEM) of WT and Δ*recA* biofilms collected on coverslips at 24 hrs. Scale bar is 3µm. **(B)** Δ*recA* biofilms withstand gentamicin treatment better than WT biofilms. Images of Crystal Violet staining of 72 hrs. mature biofilms formed by WT and Δ*recA* strains after 24 hrs. of gentamicin treatment at 3.75 µg/mL and 0.05 µg/mL. **(C)** Percentage eradication of biofilms (A595 of exposed biofilm/A595 of untreated parental biofilm) treated with a range of gentamicin concentrations for WT and Δ*recA* cells. Experiments were performed in triplicate and error bars represent standard deviation. An unpaired two-tailed T-test was performed to compare % eradication between WT and Δ*recA* strains for each concentration, * = $P < 0.05$. **(D)** Surface-attached cells with and without gentamicin treatment (15 µg/mL), were deposited on plates and CFUs were counted (representative data from biological replicate with 8 technical replicates each). Graph displays percent survival (CFU/mL) compared to the respective untreated biofilm.

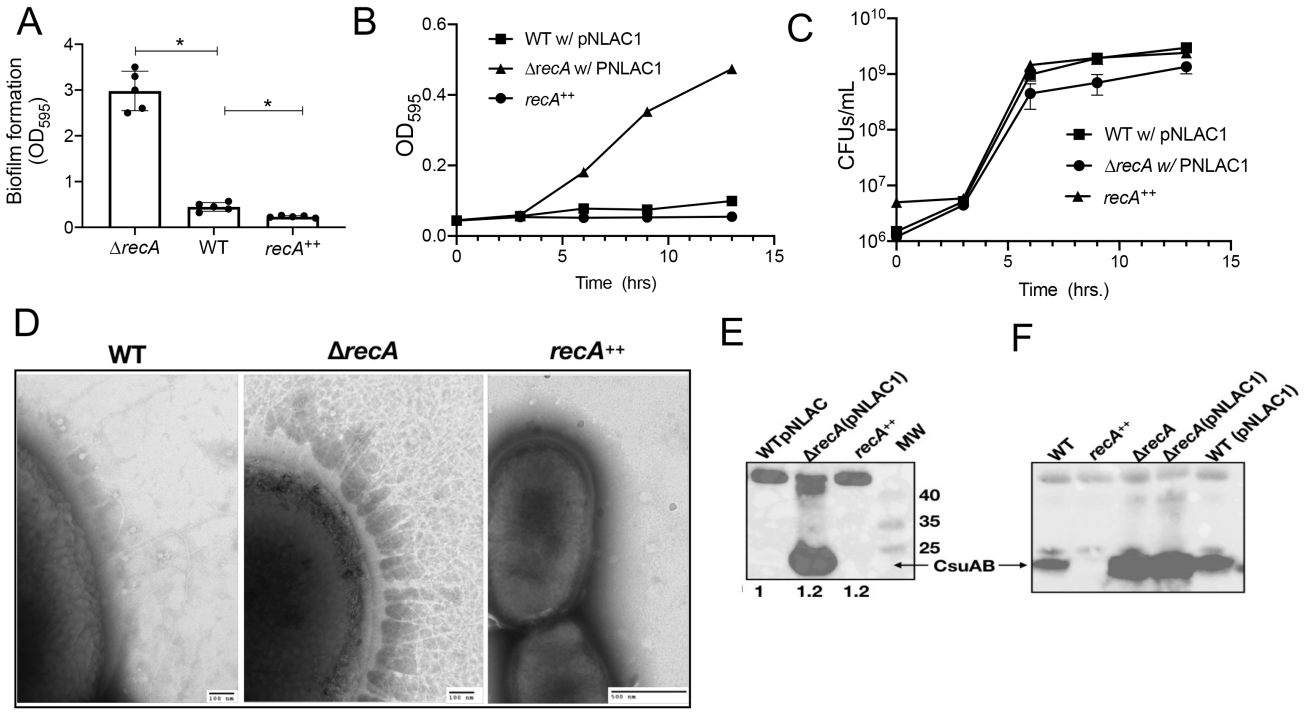

Figure 3. RecA levels modulate *A. baumannii* attachment. (**A**) Cells with high levels of RecA form significantly weaker biofilms than Δ*recA* and WT. Graph displays absorbance at 595 nm for Crystal Violet staining of polystyrene surface-adhered cells from 48 hrs. pellicles of strains Δ*recA,* WT and *recA*$^{++}$ (~4x more RecA than WT, Fig S5). Error bars represent the standard deviation of the mean. An unpaired two-tailed T-test was performed for statistical analysis. * = P < 0.05. **(B)** Δ*recA* cells attach to surfaces faster than either WT or *recA*$^{++}$. Surface attachment of the isogenic WT, Δ*recA*, and *recA*$^{++}$. All strains contain the pNLAC1 plasmid either empty or carrying the *recA* gene in *recA*$^{++}$. Error bars represent the standard deviation of the mean. (**C**) There is no large difference in growth between strains during the first 13 hrs. of biofilm formation. Colony Forming Units (CFUs)/mL of the respective strains at the same time points as in (B). The error bars represent standard deviation of the mean. Experiment was performed in technical triplicate and biological duplicate. (**D**) The Δ*recA* strain has high density of pili. Transmission electron microscopy images of the pili on the surface of the WT, Δ*recA*, and *recA*$^{++}$ strains. The scale bar for the WT and Δ*recA* strains images is 100 nm and 500 nm for *recA*$^{++}$. (**E**) Immunoblot for Csu pili isolated from the indicated strains. The total protein ratio of each cell extract from which the pili were isolated compared to WT is shown at the bottom of the image. The >40kD band is non-specific but demonstrates that similar amounts of proteins were loaded per lane. (**F**) Immunoblot for Csu pili from whole cell extracts shows the same effect as in E; there are more Csu pili in Δ*recA*. The empty vector (pNLAC1) does not affect the Csu pili as there is no difference in Csu pili between Δ*recA* cells with or without it. The cell free extracts were loaded at similar concentrations (20 µg of total protein per lane) as also shown by the >40kD band. An anti-Csu polyclonal primary antibody, and an anti-rabbit secondary antibody were used at the dilutions indicated in Materials and Methods for (E) and (F). All lanes are appropriately labelled, and the MW size markers are shown. The CsuAB protein band is highlighted by the arrows.

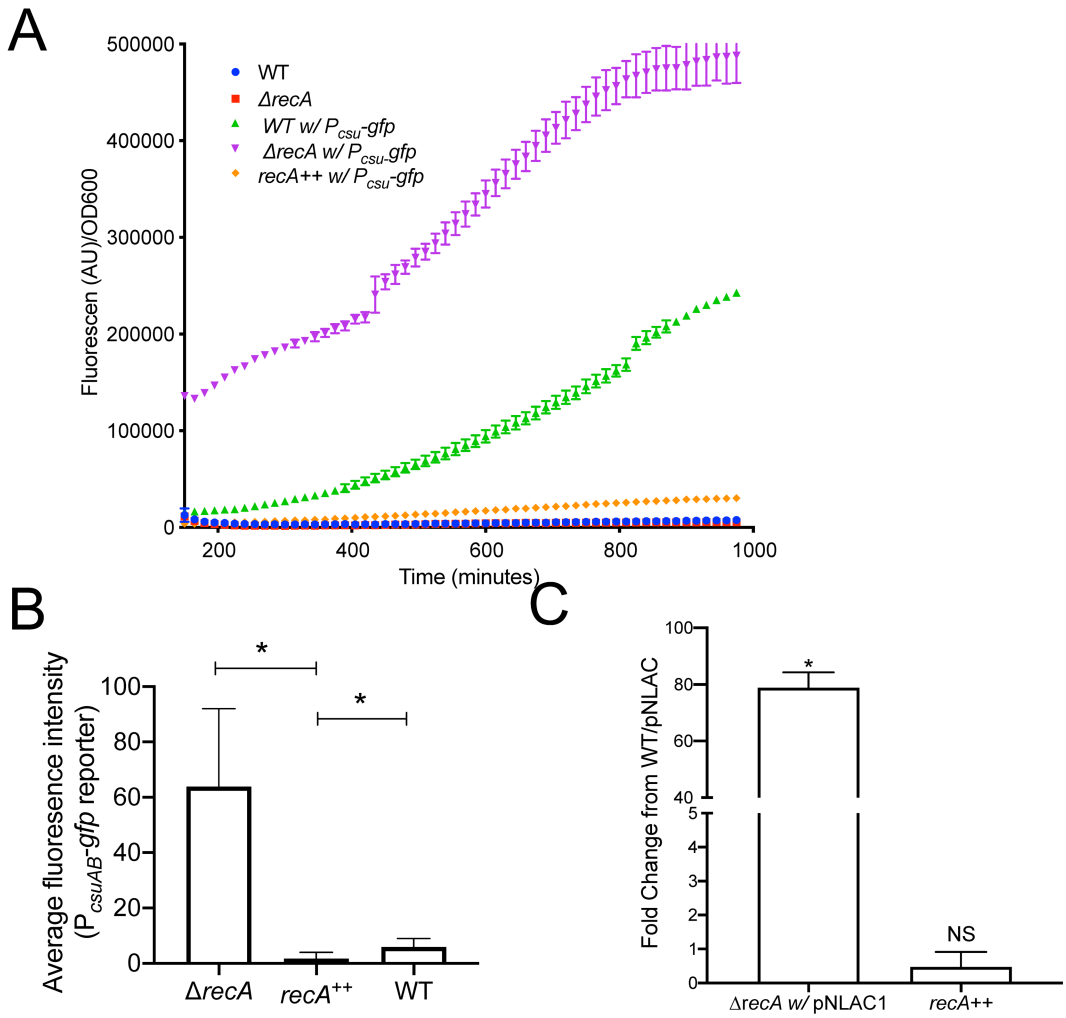

947

948 **Figure 4. Csu pili expression depends on RecA levels. (A)** Δ*recA* cells with a Csu fluorescent
949 reporter show elevated and earlier fluorescence compared to WT or *recA*$^{++}$. Fluorescence was
950 measured every 15 mins for a 1000 mins at 25ºC in static conditions in a plate reader. (**B**) Quantification
951 of fluorescence of at least 300 single cells demonstrate *csu*-gfp fluorescence dependence on RecA
952 levels; high in Δ*recA*, and low in *recA*$^{++}$. Mean single cell fluorescence with standard deviation is
953 plotted. An unpaired two-tailed T-test was performed for statistical analysis; *P<0.05 (**C**) *csu* transcript
954 is higher in Δ*recA* cells compared to WT and *recA*$^{++}$. qPCR was performed from 24 hrs. saturated
955 cultures in triplicate in three biological replicates to measure *csu* gene expression from the WT, Δ*recA*
956 and *recA*$^{++}$ strains. Expression was standardized to 16S rRNA expression, and the value for the WT
957 strain was set to 1. Error bars represent standard deviation of the mean. An unpaired two-tailed T-Test
958 was used for statistical analysis, compared to gene expression of the WT strain. *= P< 0.05, NS = not
959 significant.

960

961

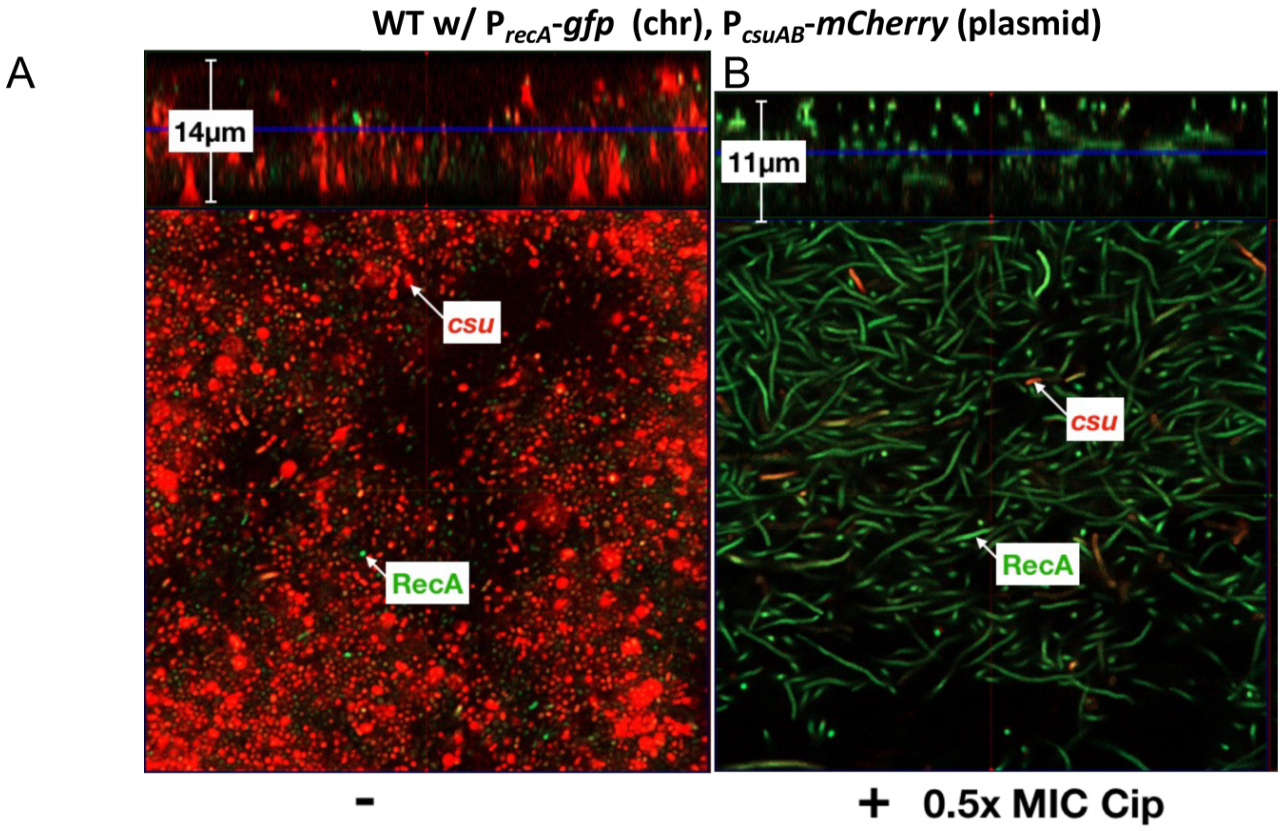

962

963 **Figure 5. High RecA levels in response to DNA damage led to thinner biofilms.** (**A**) Csu pili are
964 highly expressed in biofilm cells. Confocal microscope imaging of a double label *recA*-GFP and *csu*-
965 mCherry reporter strain. The thickness of the biofilm in the mid-Z stack is 14µm as shown in the left-
966 hand side of the figure. There are only a few RecA expressing cells. Csu and RecA cells are labeled in
967 the image. (**B**) RecA levels are high in 48 hrs. ciprofloxacin (0.5X MIC) treated pellicle biofilms. DNA
968 damaged biofilm pellicles images show elongated cells, thinning of the pellicle (mid-Z stack is 11µm)
969 and fewer *csu* expressing cells. Representative images were obtained from a Zeiss Axio Observer.Z1/7
970 with an excitation/emission of 280/618 for the red channel and of 488/509 for the green channel.

971

972

973

974

975

976

977

978

979

980

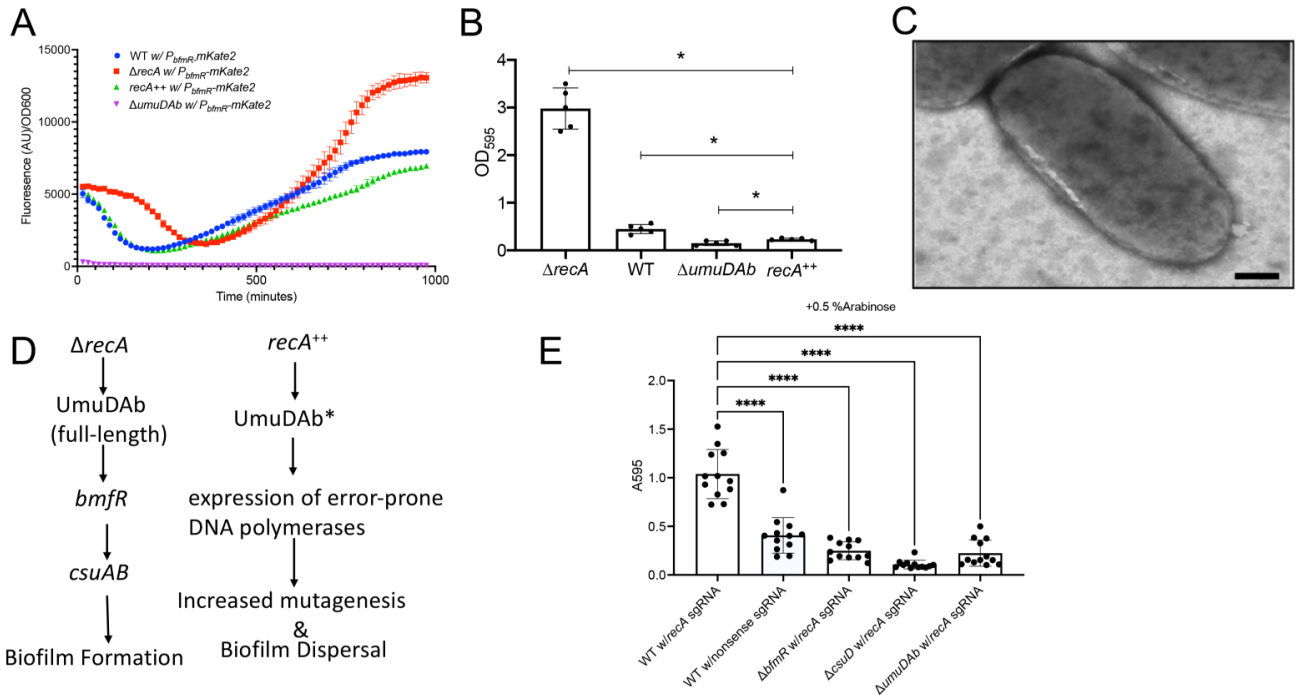

981

982 **Figure 6. RecA levels modulate biofilm development through *bfmR* and UmuDAb.** (**A**) Δ*recA* cells
983 with a *bfmR* mKate2 fluorescent reporter show earlier fluorescence compared to WT (represented by
984 the blue line), *recA*$^{++}$ (represented by the green line) or Δ*umuDAb* cells (represented by the purple line)
985 while their growth is similar. Fluorescence and OD600 were measured every 15 mins for 1000 mins
986 at 25ºC in shaking conditions in a plate reader. (**B**) A strain lacking *umuDAb* form poor biofilms
987 compared to other strains. The Δ*recA* strain forms biofilm significantly better than any of the other
988 strains tested in pairwise statistical analysis shown by the straight line on top of the columns. The WT
989 strain is significantly different to Δ*umuDAb* and *recA*$^{++}$, while Δ*umuDAb* is significantly different to
990 *recA*$^{++}$. An unpaired two-tailed T-test was performed for statistical analysis; *p<0.05. (**C**)
991 Transmission electron micrograph of the Δ*umuDAb* strain shows no evident surface pili.
992 Representative image shown. Scale bar is 100nm. (**D**) Model based on the presented data. Arrows
993 represent positive effect. **(E)** A plasmid-based arabinose inducible CRISPRi system was used to knock
994 down *recA* in WT, Δ*umuDAb,* Δ*bfmR* and Δ*csuD* cells. Graph shows absorbance at 595 nm for Crystal
995 Violet staining of polystyrene respective surface-adhered cells at 48 hrs. Experiments were performed
996 in triplicate and error bars shown represent standard deviation of the mean. An unpaired two-tailed T-
997 test was performed for statistical analysis, **** =P < 0.05.

998

999

1000

1001

1002

1003

1004 **Supplementary data (Table S1 and Figures S1-S4)**

1005 **Table S1. Strains and Oligonucleotides used in this study**

Strain	**Description**	**Reference**
A. baumannii WT	ATCC17978 Parental strain	American Type Culture Collection
A. baumannii WT *recA* GFP	ATCC17978 with chromosomal translational *recA* reporter	(Ching et al., 2018)
A. baumannii Δ*recA*	ATCC17978 *recA::km*	Gift of G. Bou(Aranda et al. 2011)
A. *baumannii* Δ*recA* complemented (Δ*rec*A (pNLAC1-*recA,* Δ*rec*A-c)	ATCC17978 *recA::km* w/ pNLAC1 *recA* (A1S_1962) promoter–*recA*, Tet^R	(Ching et al., 2017)
A. baumannii w/ pNLAC1	ATCC17978 w/ empty plasmid pNLAC1, Tet^R	This work

A. baumannii Δ*recA* w/ pNLAC1	ATCC17978 Δ*recA* w/ empty plasmid pNLAC1, Tet^R	This work
A. baumannii recA^{++}	ATCC17978 w/ pNLAC1 *recA* (A1S_1962) promoter–*recA*, Tet^R	This work
A. baumannii Δ*recA* w/pCsu GFP reporter plasmid	ATCC17978 *recA::*Km w/$Carb^R$ plasmid with a green fluorescent reporter of the Csu pilus.	This work
A. baumannii w/pCsu GFP reporter plasmid	ATCC17978 *recA::*Km w/$Carb^R$ plasmid with a green fluorescent reporter of the Csu pilus.	This work
A. baumannii recA GFP w/pCsu mCherry reporter plasmid	ATCC17978 with chromosomal GFP reporter w/$Carb^R$ plasmid with *csuAB* promoter driving mCherry, a red fluorescent reporter.	This work
A. baumannii Δ*umudAb*	ATCC17978 with a chromosomal insertion of the kanamycin gene in a 20bp deletion of the *umuDAb* gene.	This work

A. baumannii AB5075	Clinical strain of *A. baumannii*	Gift of S. Lory (Gallagher et al., 2015)
A. baumannii AB04587 *recA*::Tn	Clinical strain of *A. baumannii* AB5075 with a transposon insertion within the *recA* gene. Position 1746561. Reverse. UV sensitive.	Gift of S. Lory(Aranda et al., 2011; Gallagher et al., 2015)
A. baumannii w/ pBfmR GFP reporter plasmid	ATCC17978 w/ *pMB1-A* CarbR containing a green fluorescent reporter for *bfmR*	This work
A. baumannii ΔrecA w/ pBfmR GFP reporter plasmid	ATCC17978 *recA*::Km w/ pMB1-A CarbR containing a green fluorescent reporter for *bfmR*	This work
A. baumannii ΔumuDAB pBfmR GFP reporter plasmid	ATCC17978 *umuDAB*::Km w/ pMB1-A CarbR containing a green fluorescent reporter for *bfmR*	This work

A. baumannii recA++ w/ pBfmR GFP reporter plasmid	ATCC17978 w/ *pMB1-A* CarbR containing a green fluorescent reporter for bfmr and w/ pNLAC1 recA promoter-recA TetR	This work
A. baumannii w/ pBAD-dCas9 and nonsense sgRNA	ATCC17978 w/ *pMB2a-tet* TetR containing an arabinose inducible dCas9 and a nonsense sgRNA	This work
A. baumannii w/ pBAD-dCas9 and recA sgRNA	ATCC17978 w/ *pMB2a-tet* TetR containing an arabinose inducible dCas9 and a *recA* sgRNA	This work
A. baumannii ΔrecA w/ pBAD-dCas9 and recA sgRNA	ATCC17978 *recA*::Km w/ *pMB2a-tet* TetR containing an arabinose inducible dCas9 and a recA sgRNA	This work
A. baumannii ΔrumuDAB pBAD-dCas9 and recA sgRNA	ATCC17978 *umuDAb*::Km w/ *pMB2a-tet* TetR containing an arabinose inducible dCas9 and a *recA* sgRNA	This work

A. baumannii recA++ w/ pBAD-dCas9 and recA sgRNA	ATCC17978 w/ *pMB2a-tet* TetR containing an arabinose inducible dCas9 and a *recA* sgRNA and w/ pNLAC1 *recA* promoter-*recA* TetR	This work
A. baumannii Δ*csuD*	ATCC17978 lacking pAB3, S/T sensitive, *csuD* mutant (ATCC 17978pAB3- ΔcsuD::frt A)	(Moon et al., 2017)Gift of M. Feldman
A. baumannii Δ*bfmR* (EGA496)	ATCC17978, *bfmR* mutant	Gift of E. Geisinger
Oligonucleotides	**Sequence 5'to 3'**	
RecALICF	TACTTCCAATCCAATGCAATGGATGAGA ATAAAAGCAAAGCATTACAA	This work
RecALICR	TTATCCACTTCCAATGTTATTATTACGATT CTAATAAAAGATCTGGCTCTTC	This work
csu_f	ATTCATATGGGTCTCACTATTATCCAGCC TGTAAGTACTATTTAAAAAAAG	This work
csu_r	ATTGCATGCGGTCTCAGTACAACCTACAT ATATAATGATTAGATTTGTAGAACAA	This work

pBP_pTU_f	ATTTCAGATAAAAAAAATCCTTAGCTTTCG	This work
pBP_r	TCTTTTCGGTTTTAAAGAAAAAGGG	This work
pTU_r_insert	TGCAGCGTCTCTGGCA	This work
16S-qPCR-F	GTAATACAGAGGGTGCGAGCGTT	This work
16S-qPCR-F	GTAATACAGAGGGTGCGAGCGTT	This work
csuAB-qPCR-F	GGTGGTAGTCAAACTGAAGGA	This work
csuAB-qPCR-R	GCAACTACATCAGCAGAAGC	This work
1389 F-out	CGTAATGGTCGTGGTCGCAGCCG	This work
1389 R-out	GGGTCGAGTTCTGCCCGATAGCC	This work
1389F-Kan	CTCGCTTGGACTCCTGTTGATGGTTTCCCATCACCAGCGCAAGAT	This work
1389R-kan	AGGGCGCCCCAGCTGGCAATTCCGACGTCTAAGGAATGTGGTAAATTTTA	This work
Kan F	AGACGTCGGAATTGCCAGCT	This work

Kan R	ATCAACAGGAGTCCAAGCGAG	This work
nonsense_sgRNA_r	aaacCTGCCATACCAGGCGCGTAC	(Brychcy et al., n.d.)
nonsense_sgRNA_f	tagtGTACGCGCCTGGTATGGCA	(Brychcy et al., n.d.)
recA_ORF_sgRNA_r	aaacCTTTGAGCCAAATTGAGAAG	This work
recA_ORF_sgRNA_f	tagtCTTCTCAATTTGGCTCAAAG	This work
pBfmR_f	attCATATGGGTCTCactatgccagcatagctccat	This work
pBfmR_r	attGCATGCGGTCTCagtacatcattgcccctataaatctcattac	This work
bfmR_umuD_motif_F(Cy3)	TGTCGGGAGATAGCATACCA	This work
bfmR_umuD_motif_R	TGTTTTGTTGCATTTTATTAATCTTTG	This work
bfmR_EMSA_sequence	TGTCGGGAGATAGCATACCAAAGCTGTGAAAAAACACTTATAGATAACTTTGTGGATAACTCAAAAAACAAACACTTGAGTGAATTTAAATTTAGTGAAGAAATAATTTGTTTAATATTCATACATAGGAAATATGAATAGATTATGACATTTAAGAACAATAAATAGATAATAAAAATACCTGAAAATTCAAAGATTAATAAAATGCAACAAAACA	This work

1006

1007

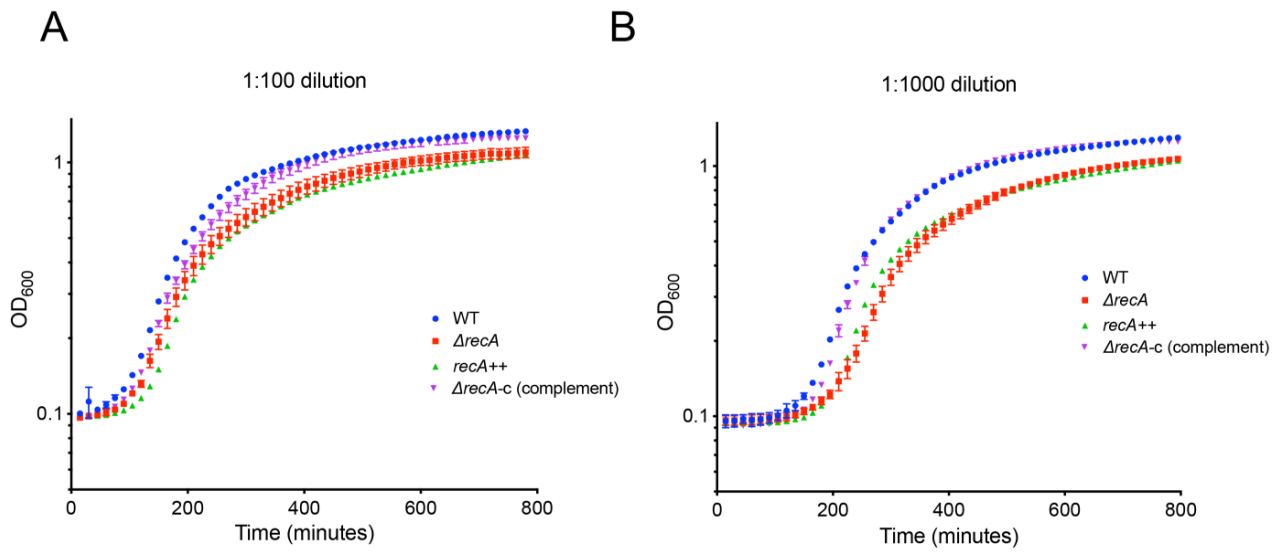

1008

1009 **Figure S1. Δ*recA* growth is fully complemented by a plasmid borne copy of *recA* under its own**
1010 **promoter.** Cells were diluted at (A) 1:100 and (B) 1:1000 in YT medium and OD600 was measured
1011 in a plate reader every 15 mins at 37ºC with shaking. Error bars represent standard deviation of the
1012 mean of three experiments.

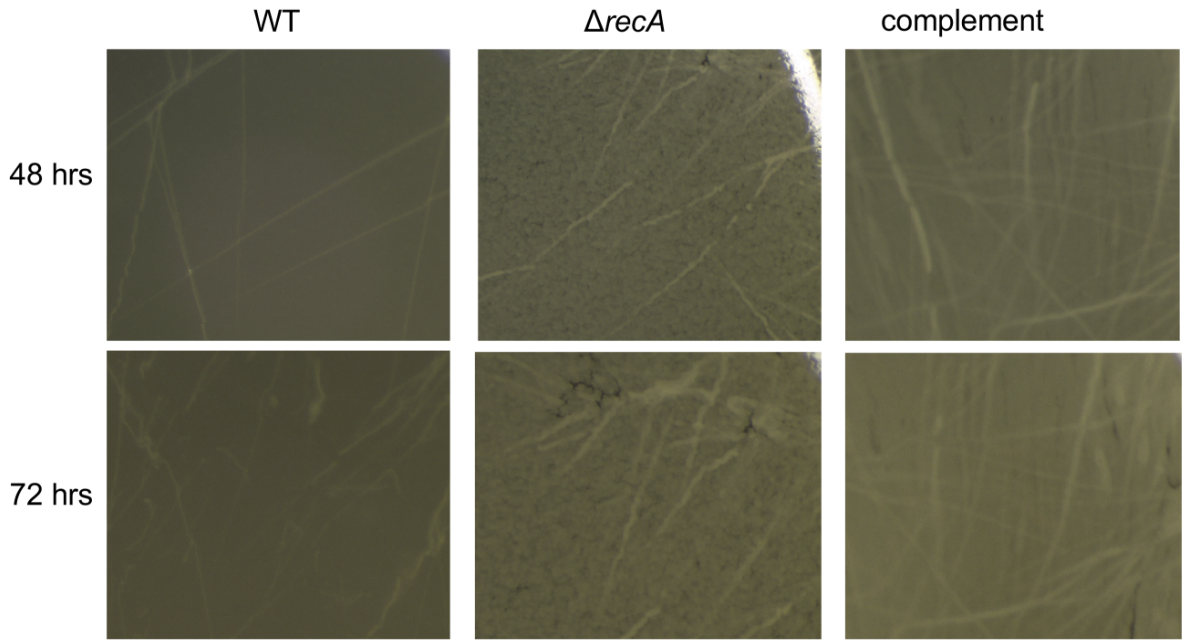

1013

1014 **Figure S2 . Δ*recA* pellicle biofilms formed at the air-surface interface have different surface**
1015 **features compared to WT.** Magnified images of the pellicle surface formed by WT compared to
1016 Δ*recA* and the complemented strain at 48 and 72 hours. The WT strain has a smooth surface with
1017 striations like complemented strain. The surface of the Δ*recA* biofilm is more granular.

1018

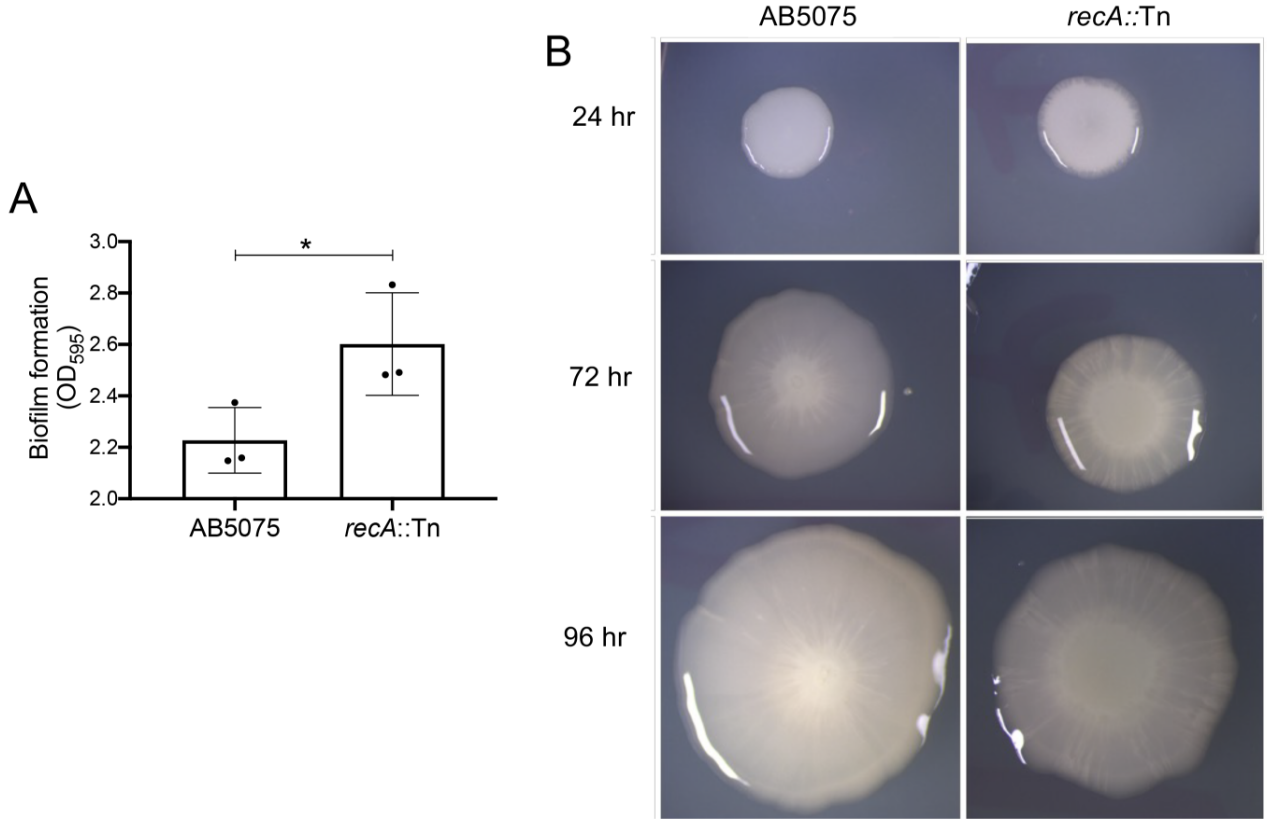

1019

1020 **Figure S3. *A. baumannii* AB5075 biofilms are influenced by RecA**. **(A)** Absorbance at 595 nm for
1021 crystal violet staining, at 48 hrs., of polystyrene-adhered AB5075 and AB5075 *recA*::Tn cells from
1022 pellicle biofilms formed in YT medium. Note the Y-axis start at 2.0. An unpaired T-Test was used for
1023 statistical analysis relative to the parental strain, *= $P < 0.05$ **(B)** Colony biofilms at 24, 48 and 72 hrs.
1024 in R2 medium with 1.5% agar instead of YT. The colony biofilms of the AB5705 *recA::*Tn have a
1025 different morphology and smaller size than the parental strain.

1026

1027

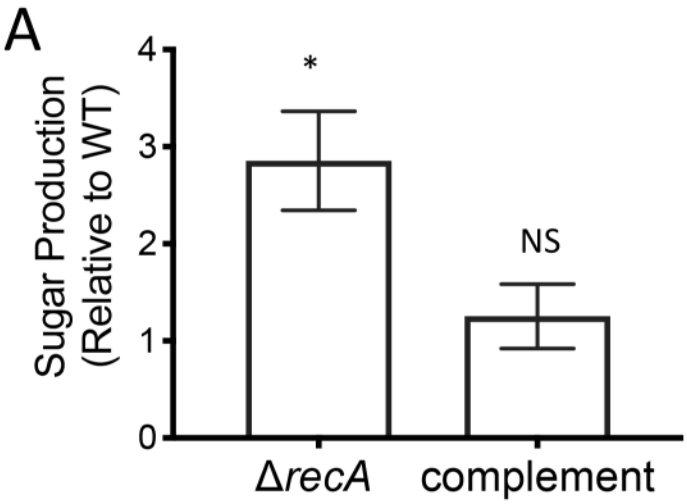

1028

1029 **Figure S4. Δ*recA* biofilms have increased observable matrix compared to WT biofilms. (A)** The
1030 matrix fraction isolated from Δ*recA* cells has a shift towards increased total carbohydrate content. Total
1031 extracellular matrix was extracted from saturated stationary phase cultures. Total carbohydrates were
1032 measured from WT, Δ*recA* and complemented Δ*recA* cells. Experiments were performed in triplicate.
1033 Error bars represent standard deviation. An unpaired two-tailed T-Test was used for statistical analysis
1034 relative to WT strain; * = P <0.05, NS = Not Significant.

1035

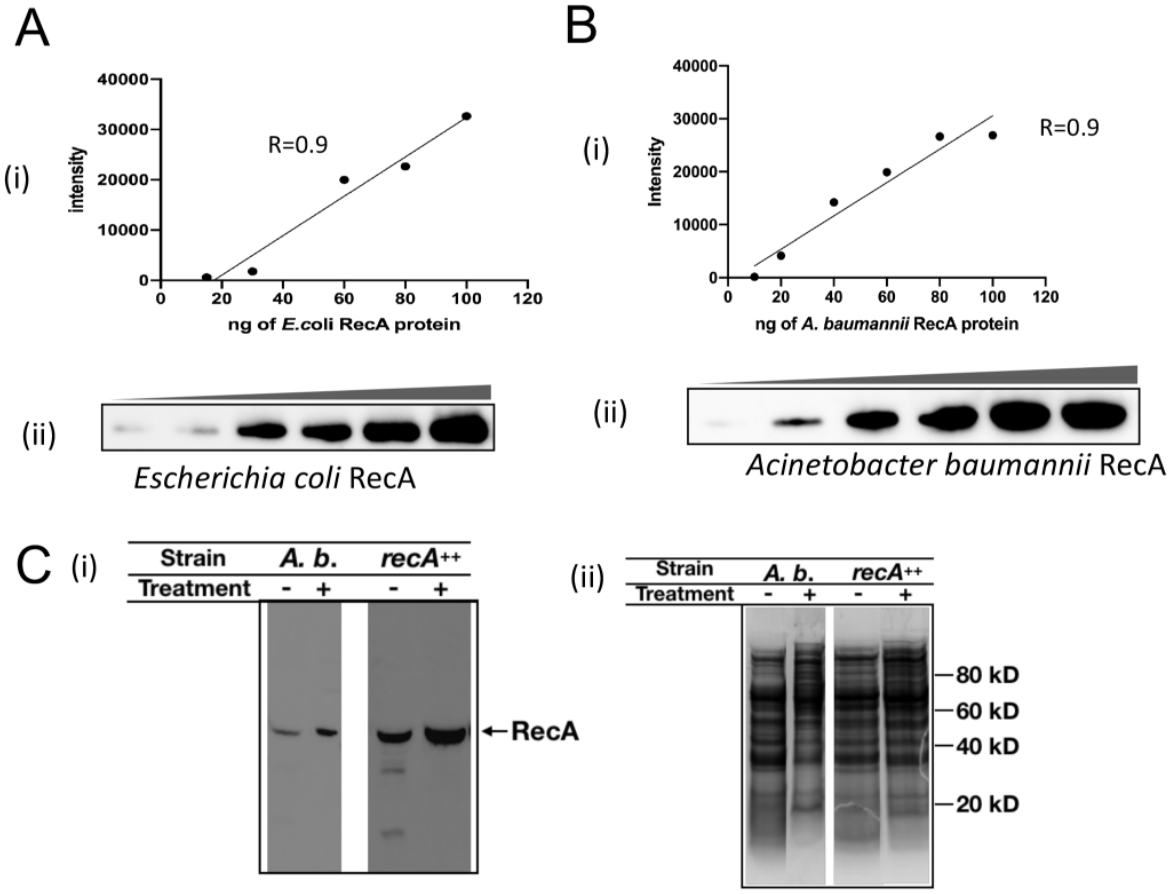

1036

1037 **Figure S5. *recA*$^{++}$ produces has 3-5-fold more RecA than WT strain**
1038 Recombinant *E. coli* RecA an *A. baumannii* RecA were purified as indicated in Materials and Methods.
1039 Increasing amounts of either protein were separated by PAGE and an immunoblot was carried out with
1040 the same dilution of anti-RecA antibody (Abcam, 1:10,000) and conditions. **(A)** (i) *E. coli* RecA
1041 standard curve (15, 30, 60, 80, 100 and 200 ng) and (**B**) (ii) *A. baumannii RecA* standard curve (10, 20,
1042 40, 60, 80, and 100 ng). No significant differences in recognition by the antibody were observed. Blot
1043 was repeated three times. Representatives immunoblot for each curve (A(ii) and B(ii)) are shown. **(C)**
1044 (i) Immunoblot for RecA of extracts of *A. baumannii* cells with (+) or without (-) 3 hr 10x MIC Cip
1045 exposure to induce the DNA damage response. Density analysis with ImageJ of the bands showed that
1046 the *recA*$^{++}$ strain has between 3-5-fold more RecA than the WT strain. The samples shown were
1047 separated in the same gel and divided electronically for figure clarity. (ii) Separation of cell free extracts
1048 of the respective samples in (i) by SDS-PAGE on a 12% Bis-Tris gel in MOPS buffer to demonstrate
1049 that similar total protein was loaded per well. Estimated molecular weight sizes are shown in the right-
1050 hand size of the gel. The calculations are the result of 4 biological replicates.

1051

1052

1053

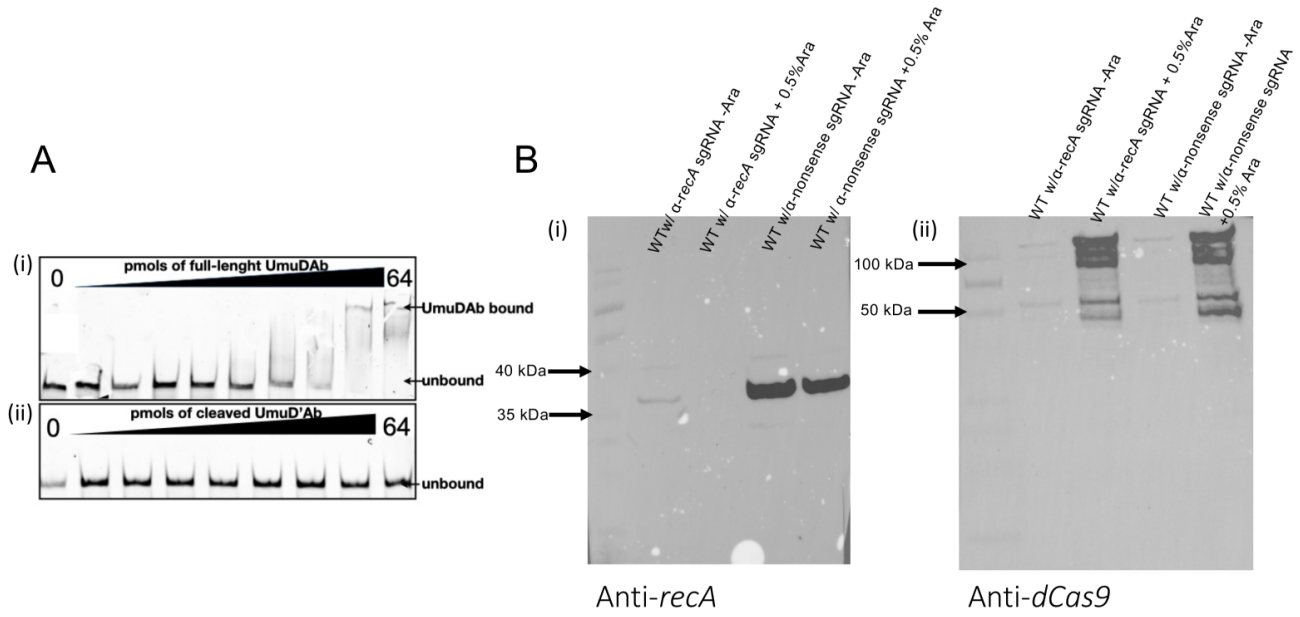

Figure S6. (A) Electrophoresis mobility shift assay (EMSA) of purified (i) full length UmudAb and (ii) cleaved UmuDAb to sequences containing the *bfmrR* promoter. The recombinant proteins were purified in *E. coli* from his-tagged versions of full length and cleaved UmuDAb. B) The plasmid-based CRSPRi we developed inhibits *recA* expression only in cells containing the sgRNA targeting the *recA* gene. Immunoblot for (i) RecA and (ii) dCas9 in CRISPRi knock down strains of WT background with *recA* and nonsense sgRNA with (+) or without (-) 0.5% Arabinose.